

# CO in distantly active comets

M. Womack<sup>1</sup>, G. Sarid<sup>2</sup>, K. Wierzos<sup>1</sup>

<sup>1</sup>University of South Florida, <sup>2</sup>Florida Space Institute, University of Central Florida

Received \_\_\_\_\_; accepted \_\_\_\_\_

## 1. Abstract

The activity of most comets near the Sun is dominated by the sublimation of frozen water, the most abundant ice in comets. Some comets, however, are active well beyond the water-ice sublimation limit of  $\sim 3$  AU. Three bodies dominate the observational record and modeling efforts for distantly active comets: the long-period comet C/1995 O1 Hale-Bopp and the short-period comets (with Centaur orbits) 29P/Schwassmann Wachmann 1 and 2060 Chiron. We summarize what is known about these three objects with an emphasis on their gaseous comae. We calculate their CN/CO and CO<sub>2</sub>/CO production rate ratios from the literature and discuss implications. Using our own data we derive CO production rates,  $Q(\text{CO})$ , for all three objects, in order to examine whether there is a correlation between gas production and different orbital histories and/or size. We further examine the applicability of existing models in explaining the systematic behavior of our small sample. We find that orbital history does not appear to play a significant role in explaining 29P's CO production rates. 29P outproduces Hale-Bopp at the same heliocentric distance, even though it has been subjected to much more solar heating. Previous modeling work on such objects predicts that 29P should have been devolatilized over a fresher comet like Hale-Bopp. This may point to 29P having a different orbital history than current models predict, with its current orbit acquired more recently. On the other hand, Chiron's CO measurements are consistent with it being significantly depleted over its original state, perhaps due to increased radiogenic heating made possible by its much larger size or its higher processing due to orbital history. Observed spectral line profiles are consistent with the development and sublimation of icy grains in the coma at about 5-6 AU for 29P and Hale-Bopp, and this is probably a common feature in distantly active comets, and an important source of volatiles for all comets within 5 AU. In contrast, the narrow CO line profiles indicate a nuclear, and not extended, origin for CO beyond  $\sim 4$  AU.

## 2. Introduction

As a typical comet approaches the inner solar system it develops a coma when frozen water begins to sublime at  $\sim 3$  AU from the Sun.<sup>1</sup> Some comets, however, exhibit measurable activity beyond this water ice sublimation boundary (Whitney 1955; Roemer 1962; Meech & Jewitt 1987; Hughes 1991; Sekanina et al. 1992), and up to a third of all comets observed become active beyond 3 AU (Mazzotta Epifani et al. 2007). Sublimation of water ice may still generate some activity beyond the normal water-ice sublimation boundary of  $\sim 3$  AU. Even at very large distances, water ice sublimation can still occur if triggered by impacts from other small bodies, tidal disruption from interactions with massive planets, and interactions with solar flares and solar wind erosion (Strazzulla et al. 1983; Stern 1995; Sekanina et al. 1994; Boss 1994). Collectively, however, these possible water-ice sublimation triggers are unlikely to generate the long-lived comae observed in most distantly active comets (Mumma et al. 1993). Thus, most comets that are active beyond  $\sim 3$  to 4 AU should be considered to have comae which are generated by a volatile other than water.

Understanding how comae are generated in comets is critical to developing accurate

---

<sup>1</sup>This is the heliocentric distance at which the sublimation temperature of water ice,  $T_{sub} \sim 150$  K, assuming a gas density of  $\sim 10^{-13}$  cm<sup>-3</sup>, (Yamamoto 1985), equals the blackbody temperature of a fast rotating spherical comet nucleus,  $T_{bb}$ , according to

$$T_{bb} = \left( \frac{1 - A}{\epsilon} \right)^{1/4} T_{\odot} \left( \frac{R_{\odot}}{2r} \right)^{1/2}, \quad (1)$$

where  $A$  = nucleus bond albedo (typically assumed to be in the range of 0.03 – 0.15),  $\epsilon$  is the surface emissivity ( $\sim 0.5$  - 0.9),  $R_{\odot}$  and  $T_{\odot}$  are radius and temperature of the Sun, respectively.

models of nucleus composition. The activity of distant comets also has important implications for other icy objects in the outer solar system, some of which may share common origins with comets. For example, some short-period comets may be collision fragments from Kuiper Belt Objects (KBOs) (Farinella & Davis 1996; Durda & Stern 2000; Schulz 2002; Dones et al. 2015). Also, KBOs, Pluto and even icy moons may also experience similar physical and chemical conditions as distantly active comets (Weissman 1999; Bockelée-Morvan et al. 2001).

Analysis of visible and infrared observations often provide useful information, such as the extended comae of distant comets are composed primarily of dust grains with a total mass of  $\sim 10^9$  kg and coma expansion velocities of  $0.3 \text{ km s}^{-1}$  or less (also see Whitney 1955; Hughes 1991; Trigo-Rodríguez et al. 2010; Kulyk et al. 2016). Visible lightcurves often show variations of two to four magnitudes over a few weeks and much smaller amplitude changes over a few hours. The larger amplitude changes are typically assumed to be due to significant mass loss; on the other hand, smaller amplitude variations are often attributed to the rotation state of the comet’s nucleus (Whipple 1980; Meech et al. 1993).

In addition to dust, gaseous emission has also been detected.  $\text{CO}^+$ , CN and OH were the first volatiles observed in distantly active comets (Cochran et al. 1980; Wyckoff et al. 1985), but they cannot drive the activity. This is because they are produced through ionization or dissociation of other molecules in the coma and do not exist in the nucleus. Observations of these species, however, are still useful as tracers of their parent molecules (Cochran & Cochran 1991; A’Hearn et al. 1984; Feldman et al. 2004). For example, spectra of OH emission may be useful in determining whether  $\text{H}_2\text{O}$  (the presumed parent of OH) is sublimating. When CN is observed, then HCN is likely to be abundant near the surface or in the coma. However, we cannot rule out a distributed source, such as  $\text{C}_2\text{N}_2$ ,  $\text{HC}_3\text{N}$  or even N-bearing refractories as a parent of CN (Feldman et al. 2004; Despois et al.

2005; Festou et al. 1998). CO is difficult to photoionize beyond 5 AU from the Sun, so detecting  $\text{CO}^+$  implies either unusual ionization of CO, or more likely, a very large amount of CO being released in the coma. Thus,  $\text{CO}^+$  may be a useful tracer of CO emission (Magnani & A’Hearn 1986; Cochran & Cochran 1991).

Carbon monoxide is of particular interest, because of its identification as a “supervolatile” (cosmogonically abundant molecules with sufficient equilibrium vapor pressures to vigorously sublime at very large ( $> 35$  AU) heliocentric distances) (see Table 1). A breakthrough in understanding distantly active comets occurred when CO gaseous emission was detected at millimeter wavelengths in comet 29P/Schwassmann-Wachmann 1 (hereafter referred to as 29P) at  $\sim 6$  AU in amounts significantly higher than the dust production rates (Senay & Jewitt 1994). Carbon monoxide was already suspected of being in 29P’s coma, because of the previously observed  $\text{CO}^+$  in 29P (Larson 1980; Cochran & Cochran 1991) and the very low sublimation temperature of CO ice; indeed, its detection in comets was predicted based on favorable excitation conditions and expected production rates (Crovisier & Le Bourlot 1983). The following year, CO emission was also detected in C/1995 O1 (Hale-Bopp) over 6.8 - 6.0 AU (Jewitt et al. 1996; Biver et al. 1996; Womack et al. 1997), and in 2060 Chiron at 8.5 AU (Womack & Stern 1999). Doubts were raised about the Chiron CO detection (Bockelée-Morvan et al. 2001); however, an independent re-analysis (Jewitt et al. 2008) maintained that the CO line was formally detected in Chiron. The derived CO production rates were high enough that CO outgassing was assumed to be the main cause of activity for all three objects (Table 2).

Other highly volatile and abundant gases, such as  $\text{CO}_2$ ,  $\text{CH}_4$ , and  $\text{N}_2$  may contribute to distant activity, but are difficult to observe (Prialdnik et al. 2004; Ootsubo et al. 2012; Reach et al. 2013a; Bauer et al. 2015a).  $\text{CO}_2$ ,  $\text{CH}_4$  and  $\text{N}_2$  do not possess an electric dipole moment and thus have no rotational transitions, which are needed for observations at

millimeter wavelengths. They have transitions at infrared wavelengths, but the emission often suffers telluric contamination and are weakly excited by solar radiation beyond 4 AU. Observations from space-based telescopes indicate that  $\text{CO}_2$  is much more abundant than CO in a large survey of distant comets (see summaries by Ootsubo et al. (2012); McKay et al. (2012)).  $\text{CO}_2$ -dominated outflows are documented in comets 103P/Hartley2 (A’Hearn et al. 2011) and 67P from spacecraft data (Hässig et al. 2015), which show that  $\text{CO}_2$  is a major player for these comets closer to the Sun. As we discuss later, all available data indicate that  $\text{CO}_2$  is not likely responsible for most of the observed activity in 29P, Hale-Bopp, and Chiron. Methane has not been detected in distant comets, although significant limits were set for 29P (see Table 2).  $\text{N}_2$  emission in comets can be estimated from optical spectra of  $\text{N}_2^+$  (Womack et al. 1992; Lutz et al. 1993; Cochran et al. 2000; Cochran 2002; Ivanova et al. 2016) and with mass spectroscopy from spacecraft data (Rubin et al. 2015). All detections, or non-detection limits, point to  $\text{N}_2$  abundances being much lower than that of CO in comets, including Hale-Bopp and 29P. In addition, the nitrogen depletion issue in comets (Cochran et al. 2000; Iro et al. 2003) make it unlikely that  $\text{N}_2$  plays a substantial role in driving distant comet activity.

Other volatiles have been detected beyond 3 AU, but their low production rates also indicate that they are unlikely to generate much of the observed distant activity. For example,  $\text{CH}_3\text{OH}$ ,  $\text{HCN}$ ,  $\text{H}_2\text{CO}$ ,  $\text{H}_2\text{S}$  and  $\text{CS}$  were identified in spectra of Hale-Bopp far from the Sun, but with production rates all significantly lower than CO production rates (Biver 1997; Womack et al. 1997).

Although most cometary studies focus on abundances from near comets, large heliocentric coverage is also needed to aid compositional studies of all comets (Dello Russo et al. 2016). Although many measurements exist of distant comets, the causes of the activity are not well understood. In this paper we summarize possible energy sources and observational

results, and make a comparative study of 29P, Hale-Bopp and Chiron. Although the dust and gas counterparts of the comae are both addressed, the main emphasis is on the volatiles (mainly CO), since they are directly involved in generating the distant activity. Studying CO’s behavior beyond 4 AU is especially important to confirm its natal contributions and study it in isolation (Pierce & A’Hearn 2010).

### 3. Proposed Mechanisms to Generate Comae Far from the Sun

Solar radiation is the most significant energy source for comets. Consequently, the heliocentric distance, albedo and seasonal effects of the nucleus all play vital roles in how the energy is balanced in a comet on the surface and in the sub-surface layers of a comet nucleus. Here we review energy sources that may play a significant role in sustained activity at large distances, such as supervolatile sublimation, crystallization of amorphous water ice, and radioactive decay.

First, we consider supervolatile sublimation and outgassing. If comet material started off very cold (such as the temperatures needed initially to maintain CO, N<sub>2</sub> or CH<sub>4</sub> in solid form), then their deep interiors may not have experienced any warming episodes, and highly volatile species can be preserved in the nucleus. Sublimation of such “supervolatile” ices can drive activity far from the Sun, and possibly beyond 40 AU for the most volatile CO. One concern raised about supervolatile ices is that severe devolatilization may have occurred due to significant heating over the  $\sim 4.6$  Gyr since the comets formed. As Kouchi & Sirono (2001) point out, however, laboratory results indicate an extremely low thermal conductivity for water ice in comets, suggesting that heating is negligible below the outer several tens of centimeters, and so extends the lifetime of supervolatiles in comet nuclei. Additionally, we point out the abundant evidence for cometary supervolatiles, as recorded by observations and space mission experiments, which show that supervolatiles are long-lived in cometary

nuclei and have not been exhausted close to the Sun or preferentially in comets that sustain more heating (such as Jupiter Family comets, which have low orbital inclinations and orbital periods shorter than  $\sim 20$  years) as compared to new comets (A’Hearn et al. 2011, 2012; Hässig et al. 2015; Dello Russo et al. 2016).

Next, we examine the amorphous water ice crystallization phase change in comet nuclei. If cometary water originates primarily from preserved interstellar grains, or from the distant outer regions of the solar disk, then it is likely to accumulate in an amorphous state (Kouchi et al. 1994; Irvine et al. 2000). Upon heating, such ice undergoes a solid phase transition to a crystalline structure. The lab-measured threshold for transition to cubic ice is  $\sim 100$  K, with another transition from cubic to hexagonal ice at  $\sim 160$  K (Laufer et al. 1987). However, only the first transition is exothermic and it involves a significant change in specific density and arrangement of ice structure, so that trapped molecules can be released. The functional form for the amorphous-crystalline transition, with 95% of the ice changing to the crystalline phase in a time (sec)  $t_c$ , was derived as

$$t_c = 9.54 \times 10^{-14} \exp(5370/T) \quad (3)$$

at a temperature  $T$  (K), for the range of 125-150 K, (Schmitt et al. 1989). Extrapolation to lower temperatures gives 120 K as the activation temperature, where the rate becomes rapid ( $\sim 1$  month). This is commonly used as a nominal crystallization temperature.

This phase transition could release enough energy, approximately  $10^9$  ergs  $\text{g}^{-1}$  (Ghormley 1968; Klinger 1981), to increase the temperature of the surrounding ice by another 45 K (Enzian et al. 1997). This, in turn, could trigger even more crystallization and sublimation, creating a runaway crystallization effect (Patashnick 1974; Prialnik et al. 1992). Accordingly, much of the outermost ice of a comet that has been heated to  $\sim 140$  K is expected to be in the crystalline form. This could mean that most, if not all, of the



comets that make repeated approaches within 5 AU <sup>2</sup> of the Sun should have crystalline water ice on the outermost layers of the nucleus.

In addition to releasing energy, this phase transition decreases the density of ice from  $\rho_a \sim 1.2 \text{ g cm}^{-3}$  to  $\rho_c \sim 0.9 \text{ g cm}^{-3}$ . This structural change releases gas molecules that were trapped in the original ice, such as CO and CO<sub>2</sub> (Bar-Nun et al. 1988; Bar-Nun & Owen 1998; Prialnik et al. 1995).

Runaway amorphous ice crystallization is modulated by the fact that laboratory studies show that exothermic crystallization occurs only for pure amorphous ice. Slight impurity levels (such as  $> 2\%$  in mol of CO in the ice matrix) in the ice are enough to reduce the effective latent heat of crystallization, thus reducing the exothermic nature of the process (Kouchi & Sirono 2001). This could result in isolated bursts, rather than crystallizing all at once. Crystallization of amorphous water ice is a mechanism included in many theoretical models of distantly active comets (e.g., Prialnik & Bar-Nun 1990a,b; Capria et al. 2000; Sarid et al. 2005). While a few other exothermic mechanisms have been suggested, such as polymerization of condensed-phase HCN (e.g., Rettig et al. 1992; Matthews 1995) and melting and dissolution of gases (Miles 2016), these processes have not been put to a quantitative test or included in a full account of the energetics involved in cometary evolution.

Radiogenic heating is an additional source of energy in distant comets that may deplete significant amounts of frozen CO and other supervolatiles from the nucleus (Prialnik et al. 1987; Haruyama et al. 1993; Prialnik et al. 1995; De Sanctis et al. 2001a). The effectiveness of this mechanism depends critically on such parameters as the diffusivity and thermal

---

<sup>2</sup>Four to five AU is the approximate heliocentric range where a nucleus is expected to reach 140K due to solar heating, see equation 1.

conductivity of the nucleus, both of which have a large range in values for the ice and silicate components. However, if the nucleus is smaller than a radius of  $\sim 10$  km, then the cooling timescale from radiogenic heating is shorter than the heating timescale. These objects would effectively get rid of the excess energy generated by radioactive decay quicker than this energy can promote a thermodynamic heating cycle on icy layers (Priyalnik & Podolak 1995; Priyalnik et al. 2008). Hence, for comets with nuclei smaller than 10km, the initial temperature is probably preserved deeper than about 100 meters.

One important concern with modeling cometary ice is that the experimental value of the thermal conductivity of water ice is  $10^4$  times lower than the theoretical value (Klinger 1980; Kouchi et al. 1992), yet both quantities have been used in models of distantly active comets. The grain packing configuration and appreciable porosity can change the thermal conductivity by orders of magnitude. It is affected by the porosity, Hertz factor (the contact area relative to cross-sectional area of material grains) and the specific thermal conductivity of the ice (what phase of ice and its level of impurity) and pores (depends on the shape and inter-connectivity of the porous space). The surface-to-volume ratio of the pores is also sensitive to the actual pore size distribution, at any given layer of the nucleus, and can vary by a few orders of magnitude (Sarid et al. 2005).

If CO sublimation generates activity in a distant comet, a simple estimate of the sublimating area,  $a$ , on the nucleus can be derived using the following equation, assuming that the nucleus is a rapid rotator

$$a = \frac{(dM/dt)r^2 L_{CO}}{F_{\odot}(1 - A)}, \quad (4)$$

where  $dM/dt$  is the total mass loss rate of CO,  $F_{\odot} = 1360 \text{ W/m}^2$ ,  $r$  is heliocentric distance in AU,  $L_{CO}$  is the latent heat of sublimation for CO, and  $A$  is the Bond albedo of the nucleus. For example, using  $dM/dt = 2000 \text{ kg s}^{-1}$  from the CO observations, this estimate gives a circular spot with an emitting radius of  $\sim 2 - 6$  km, depending on whether the CO

is released as a sublimating ice ( $L_{CO} \sim 4 \times 10^5$  J/kg), or as a trapped gas in water ice ( $L_{CO} \sim 1.5 \times 10^6$  J/kg) (Brown & Ziegler 1979), corresponding to  $< 0.1\%$  of the surface area for 29P and Hale-Bopp.

As a cautionary statement, one should consider that sometimes volatiles detected in the coma did not originate directly from the comet’s nucleus, and thus do not play a role in generating activity. For example, a source could be ice-coated grains of refractory material expelled from the nucleus (Delsemme & Miller 1971; Hanner 1981, 1984). Once in the solar radiation field, there is enough energy available (if within  $\sim 5$ -6 AU of the Sun) for the ice-coatings to sublimate. Such grains reportedly are destroyed very quickly (within 20 hours for 1 micron sized grains) once their temperatures reach  $\sim 150$ K (Lamy 1974).

Evidence for the sublimation of icy grains was seen in the emission of OH at 308 nm in comet Bowell, which was detected as the comet moved from 5 to 3 AU (A’Hearn et al. 1984, 1995). Icy grains with radii of 7 - 30 micron were determined to exist in Hale-Bopp’s coma with a median lifetime of about two days at 2.9 AU (Lellouch et al. 1998). Further evidence is found from spectral line-widths of methanol and other species in Hale-Bopp at  $\sim 5$  AU, which were much wider than one would expect for molecules sublimating directly from the nucleus (Womack et al. 1997). 103P/Hartley 2 was also observed by the EPOXI mission and the large effective sublimation area derived from photometric observations was determined to be from ice grains sublimating, but at much closer distances to the Sun (Protopapa et al. 2014; Kelley et al. 2013).

#### 4. Observations of Distantly Active Comets

In this section, we review what is known about each object, and in the next section we examine the similarities and differences between these objects and propose a common

model that may explain the distant activity.

#### 4.1. Comet Hale-Bopp

Comet Hale-Bopp presented an exceptional opportunity to study distant activity, since it already had a giant coma upon discovery at 7 AU. It is a long-period comet with a high-inclination orbit, and, thus has a very different orbital history than either 29P or Chiron. Because it has spent most of its lifetime very far from the Sun, it is probably less processed than many other comets. It is a very large comet - its nucleus radius was measured to be in the range of  $R = 20 - 35$  km (Weaver & Lamy 1997; Sekanina 1997; Fernández et al. 1999), and  $R_{Hale-Bopp} = 30 \pm 10$  km was recommended as a compromise (Fernández 2000), which we adopt for calculations in a later section. Hale-Bopp’s radius is very similar to 29P, but much smaller than Chiron.

Hale-Bopp exhibited several changes as it approached the Sun. There were reports of a swirled “jet” and a few outbursts in the dust coma from 7 to 6 AU (Sekanina 1996; Weaver et al. 1997). Multiple porcupine-like features were first observed during May-Jul 1996 at  $r \sim 4$  AU and continued for several months during perihelion approach (Boehnhardt et al. 1997; Braunstein et al. 1997; Weaver et al. 1997). Surface brightness profiles of Hale-Bopp’s coma at  $\sim 7$  AU were fit with a power law and had a slope of  $s = -0.9$  to  $-1.2$  (Weaver et al. 1997), which is consistent with a spherically symmetric outflowing coma subject to solar radiation pressure.

Numerous records were set for the detections of cometary gases at large heliocentric distances with Hale-Bopp, including the first time that  $\text{CH}_3\text{OH}$ ,  $\text{HCN}$ ,  $\text{H}_2\text{S}$ ,  $\text{CO}_2$  and  $\text{H}_2\text{CO}$  were observed in a comet beyond 4 AU (Womack et al. 1997; Biver et al. 1997b; Woodney et al. 1997; Crovisier et al. 1997). Many of these species were observed at even

larger distances post-perihelion (Biver et al. 1997b, 2002). Carbon monoxide emission was first detected in Hale-Bopp at  $\sim 6.8$  AU (Jewitt et al. 1996; Biver et al. 1996) with production rates high enough to cause the observed dust production. CO<sub>2</sub> emission was detected at 4-5 AU via its vibrational bands at  $4.3 \mu\text{m}$  and inferred from CO Cameron band emission, present at  $\sim 15\%$  of the production rate of CO (Crovisier 1997; Weaver et al. 1997). A strong upper limit was obtained for N<sub>2</sub><sup>+</sup> in Hale-Bopp near perihelion by Cochran et al. (2000), which when compared with CO<sup>+</sup> measurements is also consistent with N<sub>2</sub> produced in much smaller quantities than CO. The production rates of OH (a proxy for H<sub>2</sub>O), CH<sub>3</sub>OH, HCN, H<sub>2</sub>S and H<sub>2</sub>CO were all much lower than those of CO. We conclude that Hale-Bopp’s gas coma was dominated by CO whenever the comet was beyond 4 AU pre-perihelion (Weaver et al. 1997; Womack et al. 1997; Biver et al. 2002).

The physical state of Hale-Bopp’s coma volatiles is revealed by their millimeter-wavelength spectral line profiles. For example, CO spectra had a velocity blue-shift of  $\sim 0.4$  km s<sup>-1</sup>, and narrow line-widths of FWHM  $\sim 0.3$ - $0.4$  km s<sup>-1</sup> (Biver et al. 1996; Jewitt et al. 1996). The narrow line-widths are consistent with originating from deeper and colder regions in the nucleus. At larger distances, the CO line profile occasionally exhibited two narrow blue-shifted peaks (Womack et al. 1997; Gunnarsson et al. 2003); however, a single peak was observed most of the time. The velocity vector component of the spectra shows a sunward release of CO into the coma. The CO line-shape was different post-perihelion and exhibited a red-shifted peak along with a blue-shifted peak. The double peaks were interpreted by Gunnarsson et al. (2003) as evidence for both nuclear and extended CO sources, similar to their model for 29P.

Interestingly, beyond  $\sim 4$  AU, the spectral line profiles of most other species were significantly different from that of CO. For example, CH<sub>3</sub>OH, OH, HCN and H<sub>2</sub>S had much broader line-widths than CO, and very little, if any, velocity shifts (see Figure 1).

Their line-widths were  $\text{FWHM} \sim 0.7$  to  $1.5 \text{ km s}^{-1}$  over the range of 5 to 4 AU. Beyond 4 AU, CO linewidths were typically much narrower,  $0.4 \text{ km s}^{-1}$ , although occasionally the line was observed to be much broader (Womack et al. 1997; Biver et al. 2002). Since the spectral linewidths are mostly a result of the thermal distribution of the gas, different production mechanisms between CO and the other molecules are responsible for most of the observed variation in line profiles. The broader, cometocentric line profiles may be explained if  $\text{H}_2\text{O}$ ,  $\text{CH}_3\text{OH}$ ,  $\text{HCN}$ ,  $\text{H}_2\text{CO}$  and  $\text{H}_2\text{S}$  were first released into the coma on grains, and then sublimated when they accumulated enough energy from the solar radiation field. Volatiles released from a symmetric halo surrounding the nucleus will appear centered on the ephemeris velocity. They will also be at a higher temperature and have a larger velocity distribution (and larger line-widths) than those released directly off the nucleus. Occasionally,  $\text{HCN}$  and  $\text{CH}_3\text{OH}$  spectra mimicked the CO line profile shape, which may indicate that they were produced from two or more methods (Gunnarsson et al. 2008). Unfortunately, the  $\text{CO}_2$  band at 4.3 microns in Hale-Bopp is not spectrally resolved and, so, one cannot derive a useful upper limit to velocity information of the  $\text{CO}_2$  emission.

The pre-perihelion production rates and narrow line profiles of CO, and dust production rates, in Hale-Bopp are best reproduced by nucleus models that contain amorphous water ice with trapped CO gas, small amounts of CO ice, and crystallization of water ice starting at  $\sim 7$  AU from the Sun (Priyalnik & Podolak 1999;ENZIAN 1999; Capria et al. 2002). Prior to crystallization, sublimation of solid CO is invoked as the dominant source of activity, without detailing the source of CO ice in the nucleus. The models predict slightly higher production rates post-perihelion than pre-perihelion, which was not seen by Biver et al. (2002); Gunnarsson et al. (2003). This suggests that thermal inertia was not very important for Hale-Bopp once the comet was beyond 4 AU, and therefore most of the activity is at or near the surface of the nucleus. Observations are also consistent with the activity being well-correlated with insolation, as evidenced by symmetric behavior of gas and dust

production rates before and after perihelion (Biver et al. 2002).

## 4.2. Chiron

2060 Chiron is an unusual icy minor planet. When it was discovered in 1977, it was categorized as the most distant known asteroid. Its reflectance spectrum had a relatively neutral “color”, similar to C-class asteroids (Lebofsky et al. 1984; Hartmann et al. 1990; Stern et al. 2014), and it occasionally outbursts and develops a coma, which warrants it a formal comet designation (Tholen et al. 1988; Meech & Belton 1990). Evidence for CN and CO gaseous emission (Bus et al. 1991; Womack & Stern 1999) further secured the cometary identity.

In addition to its cometary designation, orbital dynamical studies place Chiron among the small population of large, outer solar system objects called Centaurs, which are moderately sized Kuiper Belt Objects that have moved in closer, with unstable orbits, and cross one or more giant planet orbits (e.g., Fernandez 1980; Stern 1989; Hahn & Bailey 1990; Levison & Duncan 1994; Fernandez & Gallardo 1994). Its brightness varies significantly on both short and long timescales, with changes in V and R mag of  $\sim 0.05 - 0.10$  magnitudes over hours and  $> 1.5$  mag over months and years (Tholen et al. 1988; Bus et al. 1989; Luu & Jewitt 1990; Buratti & Dunbar 1991; Duffard et al. 2002). A water-ice signature was detected in the near-infrared, which also appears to vary over time (Foster et al. 1999; Luu et al. 2000; Romon-Martin et al. 2003). It is not known whether the ice is primarily crystalline or amorphous; however, the measured color temperature (the equivalent blackbody temperature that is derived from the continuum spectrum of an object) of the nucleus is high enough (125 - 140 K) to trigger the crystallization phase change (Campins et al. 1994).

One of the most puzzling aspects of Chiron is that none of these changes are correlated well with heliocentric distance. In fact, Chiron reached peak brightness in the visible in 1989 at  $\sim 11$  AU, several years before perihelion, and it may have been even brighter than this at aphelion, 19 AU (Bus et al. 1993). For decades, the light curve was largely unexplained - other than some of the short-term variations being attributed to reflection off a rotating nucleus (Bus et al. 1989; Marcialis & Buratti 1993; Lazzaro et al. 1997). Attempts were made to fit the remaining light curve contributions with a model of amorphous water ice and a highly volatile ice, such as CO and/or CH<sub>4</sub>, with a dust mantle (Fanale & Salvail 1997), but they could not explain the lack of correlation with heliocentric distance.

Recently, however, these unusual changes in light curve and spectra have been explained as due to reflected light from a ring system circling Chiron, based on occultation data (Ortiz et al. 2015; Ruprecht et al. 2015). The proposed rings can account for most of the short- and long-term brightness variations, largely by a change in their orbital tilt, if the ring particles have a different albedo than the surface. This may also explain the observed changes in the water-ice spectra, provided the ice is in the rings and not on the surface. Interestingly, another large Centaur, Chariklo, has a ring system, and similar changes are noted there (Duffard et al. 2014). If confirmed in Chiron, this suggests a paradigm shift, where rings may be commonly found around Centaurs and perhaps other large icy objects, like Kuiper Belt Objects, and rings need to be included as possible contributors to observed differences among KBOs. We note, however, that the Pluto system does not have any rings and the New Horizons project searched very thoroughly for them. So, while rings could be contributors, for some of our best examples of KBOs, rings are not present.

The evidence is very strong for a model where most of Chiron’s brightness changes are due to the changing orbital tilt of a ring system and nucleus rotation; however, these cannot explain the occasional outbursts and development of a coma. One possibility is that the



rings and coma may even be interdependent, as the most likely formation mechanism for the rings is proposed to be a debris disk fed by some cometary activity, with a possibility that in-falling material from the rings could trigger outbursts (Ruprecht et al. 2015). If instead of rings, Ruprecht et al. (2015) also raise the possibility that narrow jets may generate activity by a low-gravity analog to the geyser-like vents that are sometimes observed on Neptune’s large satellite Triton or on Pluto, fueled by sub-surface geological activity. More observations are needed of Chiron, in and out of outburst, to confirm the rings or jets.

Chiron’s outbursts and coma occur at distances from the Sun too far to be caused by  $\text{H}_2\text{O}$  and  $\text{CO}_2$  ice sublimation, the drivers of most normal comets near the Sun. Instead, the outgassing activity is probably largely due to the sublimation of even more volatile species. CO is the most likely candidate. Its emission in Chiron was singularly detected via the 1-0 rotational line in 1995 with production rates high enough to drive the observed dust coma (Womack & Stern 1999; Jewitt et al. 2008). The measured CO production rate indicates that much less than 1% of Chiron’s surface was active in 1995, consistent with CO-driven vents or geysers.

Occultation and thermal emission measurements indicated that Chiron has a very large diameter, ranging from  $D = 150 - 220$  km (Campins et al. 1994; Elliot et al. 1995; Bus et al. 1996; Fernández 2000). Following the discussions by Groussin et al. (2004) and Fornasier et al. (2013), we recommend a diameter of  $D_{\text{Chiron}} = 218 \pm 20$  km, which we use for later calculations. Chiron’s nucleus is clearly larger than those of Hale-Bopp and 29P, and significantly larger than most comet nuclei.

Chiron has a low, but steady dust production rate of  $\sim 0.5 \text{ kg s}^{-1}$ , with a mean speed of  $\sim 100 \text{ m s}^{-1}$  for a coma that is populated by 1-micron sized grains, according to analysis of near-infrared H- and R-band observations (Luu & Jewitt 1990). On the other hand, modeling of V-band images indicated that the coma was dominated by much larger

100-micron sized dust grains that were largely un-sampled by the near-infrared data (West 1991; Fulle 1994; Romon-Martin et al. 2003). The larger grain sizes lead to a much higher mass loss rate of  $20 \pm 10 \text{ kg s}^{-1}$ , and slower dust expansion velocities of  $\sim 5$  to  $10 \text{ m s}^{-1}$ . This is a very low dust production rate when compared to 29P or Hale-Bopp.

Interestingly, Chiron’s color temperature measurements are 40 - 50 K warmer than expected for its nucleus if one assumes an equilibrium temperature for a fast rotator spherical blackbody. It is not known whether the aforementioned ice is primarily crystalline or amorphous; however, the measured color temperature of the nucleus is high enough (125 - 140 K) to trigger the crystallization phase change (Campins et al. 1994). Unlike 29P, Chiron’s nucleus rotation period is well determined to be  $5.917813 \pm 0.000007$  hours (Marcialis & Buratti 1993).

Information about Chiron’s gas coma is scarce. Thus far, CN and CO are the only species seen in the coma, and both were detected only once (Bus et al. 1993; Womack & Stern 1999). The optical CN detection of  $\sim 4 \times 10^{25} \text{ mol s}^{-1}$  at 11 AU correlates to a high production rate for a comet at 11 AU, and  $>4$  times greater than Hale-Bopp at 10-12 AU (Rauer et al. 2003). Emission from CN was searched for when Chiron was near perihelion at  $\sim 8.5$  AU, and was not detected down to a limit that is  $\sim 25\%$  lower than what was observed at 11 AU (Rauer et al. 1997). Chiron was reported to be undergoing an outburst during both observing runs, so it is puzzling that CN was detected only once. Thus, the CN production in Chiron may be variable and not well-correlated with either the dust production rate or heliocentric distance. The millimeter-wavelength CO detection in Chiron is consistent with a production rate of  $\sim 10^{28} \text{ mol s}^{-1}$  at 8.5 AU (Womack & Stern 1999), which is also similar to Hale-Bopp at the same distance (Biver et al. 2002), see Figure 2. The observed CO line-width was very narrow and similar to what has been observed for 29P and Hale-Bopp. The CO line-width was  $\text{FWHM} = 0.39 \text{ km s}^{-1}$ ; however,

the line was not resolved, and this should be considered an upper limit to the true spectral line-width. The narrow line width is indicative of emission from a cool gas,  $T < 110$  K, and is also consistent with a dusty CO coma, in which dust heats gas in the near-nucleus region, resulting in terminal gas velocities of  $\sim 0.4$  km s $^{-1}$  (Boice & Huebner 1993).

An upper limit of  $Q(\text{CO}) < 2 \times 10^{27}$  mol s $^{-1}$  was obtained over five observing runs from Mar 1998 - Jul 2000, when Chiron was 9 - 11 AU (Bockelée-Morvan et al. 2001). This limit is almost ten times lower than the production rate measured several years earlier by Womack & Stern (1999). Hence, the CO detected in 1995 may have been the result of an outburst and not caused by any long-lived activity from Chiron, a conclusion also reached by Bockelée-Morvan et al. (2001).

A detailed study by Fornasier et al. (2013) determined that a gas production rate of at least  $1\text{-}10 \times 10^{27}$  s $^{-1}$  were needed to drive dust production rates derived from optical observations of the coma. This amount is consistent with the CO production rate measured at 8.5 AU and comparable to upper limits derived from  $\sim 9\text{--}11$  AU. Fornasier et al. (2013) also raise CO $_2$  as capable of driving the observed dust activity. Unfortunately, there are no detections or upper limits to CO $_2$  production rates in Chiron.

The high color temperature of Chiron’s nucleus and the CO and dust production rates are predicted by two models with a highly porous nucleus containing dust and gas-laden amorphous water ice with more volatile ices deeply buried (Prialnik et al. 1995; Capria et al. 2000). In these models, crystallization of amorphous ice in the nucleus is proposed to occur near the surface, which then releases the trapped CO gas. This may be the preferred mechanism, since at the surface temperature of Chiron (120K, see Campins et al. 1994) CO and CO $_2$  ices would not survive shallower than a few skin depths (1 skin depth is  $\sim 20$  m, assuming a density of 0.7 g/cm $^3$ , see Prialnik et al. 2008). Thus, such solid ice phases of these volatile species can be ruled out as significant constituents of the top surface layers,

and are probably restricted to deeper sections of the nucleus.

### 4.3. Comet 29P/Schwassmann-Wachmann 1

Comet 29P/Schwassmann-Wachmann 1’s coma has been documented for 90 years. The comet appears to be nearly always active with numerous reports of dramatic outbursts of 4 to 8 magnitudes over relatively short time periods (e.g., Roemer 1958, 1962; Whipple 1980; Hughes 1991; Trigo-Rodríguez et al. 2010). Originally classified as a short-period comet, it has a low inclination orbit, and its heliocentric distance ranges between  $5.7 < r < 6.3$  AU. Its current orbit is nearly circular ( $e = 0.04$ ) and is relatively near the water ice sublimation zone. Dynamical studies show that 29P’s orbit has become more circular over time, and it probably only recently transferred to this orbit from one much farther from the Sun, possibly the Kuiper Belt. It is often considered to have a Centaur orbit (e.g., Fernandez 1980; Stern 1989; Levison & Duncan 1994; Fernandez & Gallardo 1994).

A recent study of 29P’s nucleus radius derives  $R_{29P}=30.2^{+3.7}_{-2.9}$  km (Schambeau et al. 2015), which we use for later calculations in this paper. This puts 29P at about the same size as Hale-Bopp and much smaller than Chiron. 29P’s large asymmetrical dust coma often exceeds 400,000 km across, and spiral structures often seen in the coma are consistent with one or more active areas on the nucleus (Roemer 1958; Whipple 1980; Cochran et al. 1982; Reach et al. 2013a). Optical imaging techniques implied that the dust coma had a surface brightness profile (see Eq. 1) of  $s = -1$  to  $-1.5$  (Meech et al. 1993; Jewitt 1993), consistent with a steady-state, uniformly outgassing coma subject to some solar radiation pressure. Jewitt (1990) estimated a dust mass loss rate of  $10 \text{ kg s}^{-1}$  and dust expansion velocity of  $200 \text{ m s}^{-1}$  from images. However, this may be an underestimate of the total mass loss, since the reflected light is dominated by light scattered by grains with sizes comparable to the observed wavelength. As a result, this technique may undercount larger

grains, which probably play an important role in the comet’s mass loss. One model of the grain size distributions indicates a much higher mass loss rate of  $\sim 600 \text{ kg s}^{-1}$  (Fulle 1992).

CN is often the first emission feature detected in optical spectra of comets far from the Sun, so it was a surprise when  $\text{CO}^+$  was the first gaseous species seen in 29P (Cochran et al. 1980).  $\text{CO}^+$  emission in 29P was initially believed to be explained by photoionization of CO; however, the lifetime for this process at 29P’s distance from the Sun (Larson 1980; Cochran & Cochran 1991) is too long to account for the observed column densities.<sup>3</sup> Collisional ionization of CO from high energy solar wind electrons has been proposed, instead, to explain formation of the  $\text{CO}^+$  in 29P (see Cochran & Cochran 1991). CN was eventually detected in 29P in Dec 1989 with a line strength weaker than the neighboring  $\text{CO}^+$  lines (Cochran & Cochran 1991; Cook et al. 2005).

The rotational period of 29P’s nucleus is unknown, with measurements ranging from 14 hours to longer than two months (Miles 2016; Ivanova et al. 2015; Moreno 2009; Meech et al. 1993; Stansberry et al. 2004; Jewitt 1990; Whipple 1980). The large uncertainty in 29P’s rotation period is a significant problem for constraining outgassing models. Since 29P’s orbit has a very low eccentricity, the surface experiences a nearly constant rate of heat forcing (and cooling rate). Thus, the variations in illumination for any given patch on the surface are predominantly a function of period and obliquity. The co-latitude and co-longitude dependence drives the sub-surface activity (neglecting lateral heat conduction). The uniqueness of 29P’s activity pattern may be the result of its relatively circular orbit

---

<sup>3</sup>The lifetime against photoionization for CO at 29P’s distance ranges from 3 - 8  $\times 10^7$  sec, depending on the solar activity (Fox & Black 1989). At the average rate of  $5 \times 10^7$  sec, CO molecules moving at  $0.45 \text{ km s}^{-1}$  away from the nucleus would travel  $\sim 0.1 \text{ AU}$  from the comet before being photoionized, which is well beyond the region where  $\text{CO}^+$  is observed (Festou et al. 2001).

and a non-simple spin state (possibly a very slow rotator with a highly oblique spin pole).

The first direct evidence for a volatile that could generate a coma in 29P was the detection of CO gas (Senay & Jewitt 1994). A production rate of  $Q(\text{CO}) = 3.0 \times 10^{28}$  molecules  $\text{s}^{-1}$  was derived, which corresponds to a mass loss rate of  $\sim 2000 \text{ kg s}^{-1}$ . Since this is much greater than the dust mass loss rate of 10 - 600  $\text{kg s}^{-1}$ , it is assumed that CO is driving the observed activity. Upper limits of  $Q(\text{CH}_4) < 1.3 \times 10^{27} \text{ mol s}^{-1}$  ( $< 5\%$  of CO) were determined from infrared spectra of 29P (Paganini et al. 2013).

Similarly, sensitive upper limits to  $\text{CO}_2$  emission show that this species is not dominant in 29P’s coma with  $Q(\text{CO}_2) < 80 Q(\text{CO})$  (Ootsubo et al. 2012; Reach et al. 2013a; Bauer et al. 2015a). We conclude that  $\text{N}_2$ ,  $\text{CH}_4$  and  $\text{CO}_2$  are produced in minor amounts when compared to CO. Comet 29P seemingly always has at least a minimal CO production, of  $Q(\text{CO}) \sim 3 \times 10^{28} \text{ mol s}^{-1}$ , which is often referred to as the quiescent or non-outbursting state (Festou et al. 2001).

Sporadic outbursts also occur which increase the comet’s CO production by up to a factor of seven (see Figure 2), even though the comet’s orbital distance does not change very much during this time. Clearly, CO outgassing is tied to the outbursting mechanism in 29P. Surprisingly, no correlations were found between observed  $\text{CO}^+$  emission and the outbursting state, as evidenced by optical observations of the coma. The production mechanism for  $\text{CO}^+$  in this comet is not clear (Cochran et al. 1980, 1982). Simultaneous observations of CO and  $\text{CO}^+$  are needed to better understand coma chemistry.

The CO activity in 29P was proposed to be released from a relatively small active area on the surface by Senay & Jewitt (1994), either by sublimation of CO, or as trapped in water ice. However, detailed models of frozen CO sublimating (whether pure or adsorbed onto water ice) does not reproduce the observations well (i.e. Enzian et al. 1997) and the surface is too warm for CO ice to survive for very long. Different models exist that

incorporate energy provided by HCN polymerization and the crystallization of amorphous water ice (Gronkowski & Smela 1998) or melting and dissolution of gases (Miles 2016); however, they do not include a full account of the energetics, so these models are of limited value. Moreover, the dust outflow velocities predicted are approximately three times lower than what was measured from HST WFPC2 imaging data (Feldman et al. 1996). The model which best explains the CO production rates to date is one that includes crystallization of amorphous water ice with trapped CO gas and pockets of CO ice, a highly tilted rotation axis and surface erosion (Enzian et al. 1997). In this model, CO production primarily comes from release as a trapped gas when crystallization occurs in amorphous ice in the sub-solar area. This model also explains outbursts with surface erosion where dust grains are released from the ice-dust matrix by the escaping gas.

Further clues about the physical state of the coma are given by the millimeter and infrared spectra of CO. The CO spectral line shapes in 29P (in both the quiescent and outbursting states) are frequently characterized by two very narrow (FWHM line-width  $\sim 0.10$  to  $0.15 \text{ km s}^{-1}$ ) velocity components, which are found at  $\sim +0.5 \text{ km s}^{-1}$  and  $-0.3 \text{ km s}^{-1}$  with respect to the cometocentric velocity (Crovisier et al. 1995; Biver et al. 1997a; Festou et al. 2001; Gunnarsson et al. 2002, see Figure 3). Two emitting regions have been proposed to explain the double-peaked (red and blue-shifted) CO line profile: a day-side and night-side region (Crovisier et al. 1995). In contrast, the two peaks are interpreted by (Crifo et al. 1999) as due to temperature distributions on the surface, and not the spatial location of vents. Still another idea is that the line-shape may be partly due to under-sampling the CO emitting region, which would preferentially detect the gas with the greatest Doppler shifts (Festou et al. 2001). Finally, the two lines could be caused by two different sources of CO: a nuclear and an extended source originating from icy grains in the coma (Gunnarsson et al. 2002).

Raster (point-by-point) mapping data with the SEST 15-m telescope indicated that there was a substantial secondary source of CO in the coma, which was hypothesized as being due to the release of CO from icy grains in the coma in 29P (Festou et al. 2001; Gunnarsson et al. 2002). In this scenario, the sunward emission from the nucleus gives a strong blue-shifted peak, and the isotropic emission of the extended source gives a so-called “horned” appearance due to under-sampling of the icy grain emission source by the radio beam. The blue-shifted part of the “horn” is blended with the sunward peak. With this model, the extended source produces  $\sim 3$  times the amount of CO as the nuclear source and is the dominant source of CO emission.

Subsequent mapping of CO emission with the IRAM 30-m dish did not show evidence for such a widespread secondary source (Gunnarsson et al. 2008). However, the data showed an asymmetric localized feature in the coma with “excess emission. This is evident in both the dust and gas comae and extends 0.5 to 2 arcminutes south of the nucleus (Schambeau et al. 2015; Gunnarsson et al. 2008), which corresponds to a projected distance starting at  $\sim 1.1 \times 10^5$  km from the nucleus (we find that the published number in Gunnarsson et al. (2008) is too high by a factor of ten). This is sometimes also referred to as a jet feature. Thus, it is possible that 29P split off a smaller piece or fragment during 2003 - 2004. Interestingly, CO emission was detected from both the main and fragment sources by Gunnarsson et al. (2008). The fragment was found to have a slightly smaller blueshift (-0.18 km/s) than the main nucleus component (-0.35 km/s). The spectral line profile of the secondary also showed the classic horned appearance, consistent with the spectra obtained at the primary position. Follow-up high angular resolution spectral mapping, or interferometry, would be invaluable for studying this “excess emission” phenomenon in 29P.

The true nature of this enhanced CO emission region in the coma is not known. A long lasting, but largely hidden, fragment or secondary component could be an important



additional source of CO in 29P’s coma (Gunnarsson et al. 2008). A secondary component would also complicate efforts to measure the rotation period of the main nucleus, which has so far remained undetermined.

We note that 174P/Echeclus, another Centaur that is sometimes active, reportedly had a distinct secondary source, which may have recently split from the primary nucleus (Rousselot 2008; Fernández 2009). This secondary extended emission in Echeclus was at a similar distance from the nucleus: the angular separation is a factor of  $\sim 3$  times, and the derived spatial separation is  $\sim 1.5$  times that of 29P’s excess emission (calculated from Rousselot 2008; Gunnarsson et al. 2008) using the correct distance (see previous paragraph). Processes acting at 29P may be similar to those at Chiron, the other Centaur in this study, producing secondaries and rings.

Infrared and millimeter wavelength spectra also showed that the CO inner coma gas in 29P is at an extraordinarily low rotational temperature of  $\sim 5\text{K}$  (Gunnarsson et al. 2008; Paganini et al. 2013), making it one of the coldest gases known in the the solar system. As discussed in Gunnarsson et al. (2002); Paganini et al. (2013), if CO molecules start out from the nucleus with  $T_{rot} \sim 5\text{K}$ , they will change excitation conditions over time and reach fluorescence equilibrium within  $\sim 2$  days. Therefore, many millimeter wavelength observations with larger beamwidths are recording spectra from molecules which are close to fluorescence equilibrium with a higher rotational temperature of 10-15K.

29P’s coma is predicted to have a significant amount of water due to the sublimation of icy grains, if water ice is present at the surface and if grains are ejected (Crifo et al. 1999). Initially, searches showed no water down to a limit of  $Q(\text{OH}) < 2\text{-}3 \times 10^{28} \text{ mol s}^{-1}$  (Cochran & Cochran 1991; Feldman et al. 1996). 29P was observed with the Herschel Space Observatory, and preliminary results claim a detection of water and HCN with line profiles that are consistent with being emitted from icy grains in the coma, but no values

have been published yet for the production rates (Bockelee-Morvan et al. 2010, 2014).

## 5. Discussion and Comparison of Distantly Active Comets

In this section, we review the similarities and differences in the observational data of Hale-Bopp, 29P and Chiron, and discuss the models that best fit these data. We focus on the spectroscopic results, mainly production rates and line profile characteristics. Representative production rates of important species in 29P, Chiron and Hale-Bopp are summarized in Table 2. In particular, we 1) examine the production rate ratios of  $CN/CO$  (and  $HCN/CO$ ) and 2)  $CO_2/CO$ , 3) discuss clues from spectral line profiles of volatile species, and 4) recalculate CO production rates for all 3 comets with consistent modeling assumptions. We then 5) summarize observational constraints to models of distant activity and 6) analyze  $Q(CO)$  for all three objects when adjusted for nucleus size and heliocentric distance.

### 5.1. Production Rate Ratios: $CN/CO$ and $HCN/CO$

CN and CO are the only gaseous species observed in all three comets, and we briefly compare their relative production rates to test models of CN and HCN in comae and to assess whether HCN is a likely competitor for triggering activity in these objects. Using values from Jewitt et al. (1996); Fitzsimmons & Cartwright (1996); Rauer et al. (1997); Biver et al. (2002), we calculate that the ratio  $Q(CN)/Q(CO)$  was  $\sim 0.003$  in Hale-Bopp at  $\sim 6.8$  AU pre-perihelion, and the same value at 4.6 AU post-perihelion (see Table 3). We derive the ratio  $Q(HCN)/Q(CO) \sim 0.004$  at 6 AU post-perihelion using values from Rauer et al. (1997); Biver et al. (2002). Interestingly,  $Q(HCN)/Q(CO) \sim Q(CN)/Q(CO)$ , even at somewhat different heliocentric distances. This is consistent

with work by Rauer et al. (2003); Fray et al. (2005); Bockelée-Morvan et al. (2008), which conclude that Hale-Bopp’s CN largely originated from HCN photolysis. Additionally, it is clear that HCN was produced in much smaller amounts than CO in Hale-Bopp at large heliocentric distances, and thus does not compete with CO in triggering activity.

Unfortunately, it is not clear what the CN/CO production rate ratio is for Chiron, because CN and CO were not measured at the same time. However, if we use the CN value at 11 AU and CO measurement at 8.5 AU, we get a similarly low value of  $Q(\text{CN})/Q(\text{CO}) \sim 0.003$ . However, we stress that these were not simultaneous measurements for Chiron, and hence the ratio is probably of limited value.

CN is only rarely observed in 29P and, when seen, it appears depleted with respect to CO, when compared to Hale-Bopp, which we use as a proxy for an unprocessed new comet. Using the CN production rate from Cochran & Cochran (1991) and the average non-outbursting value of  $Q(\text{CO}) \sim 3 \times 10^{28}$  for 29P, we calculate a production rate ratio  $Q(\text{CN})/Q(\text{CO}) \sim 0.0003$ , which is almost ten times lower than what is derived for Hale-Bopp at 4 and 6 AU. By this metric, 29P appears to have much less CN (and presumably HCN) than CO when compared to Hale-Bopp and possibly also Chiron. As mentioned previously, 29P was observed with the Herschel Space Observatory, and preliminary results claim detections of  $\text{H}_2\text{O}$  and HCN (Bockelée-Morvan et al. 2010, 2014). Once HCN production rates are published from these Herschel data, they will be useful for comparing with measured CO and CN production rates to test models of release of all three species from the nucleus (McKay et al. 2012). It will be also interesting to see whether the Herschel data support CN arising from HCN in 29P. The relative amounts of HCN and CO produced from 29P could provide clues to the comet’s formation environment. For example, if HCN and CO are both incorporated into amorphous ice, and if the cometary material was predominantly from regions where CO was more likely to be adsorbed onto forming

grains of amorphous water ice, then HCN depletion would indicate Kuiper Belt formation distances, rather than closer-in Saturn distances.

## 5.2. Production Rate Ratios: $\text{CO}_2/\text{CO}$

Another important marker in comae is the relative amount of  $\text{CO}_2$  and  $\text{CO}$ , which is a useful test of thermal evolution and/or formation models (Feldman et al. 1997a; Belton & Melosh 2009; A’Hearn et al. 2012). Although recent surveys show that  $\text{CO}_2 \gg \text{CO}$  for most comets (Ootsubo et al. 2012; Reach et al. 2013b; Bauer et al. 2015b),  $\text{CO}$  drives the activity for Hale-Bopp (beyond 4 AU) and 29P. Indeed, these two comets appear to be “CO-rich” when compared to most other comets.

$\text{CO}_2$  was directly detected in Hale-Bopp’s coma at 4.3 microns using the Infrared Space Observatory at 4.6 AU pre-perihelion and 4.9 AU post-perihelion (Crovisier 1997).  $\text{CO}_2$  was also indirectly detected in Hale-Bopp with similar values via  $\text{CO}$  Cameron band emission. These  $\text{CO}$  bands predominantly arise from  $\text{CO}_2$  dissociation (Weaver et al. 1997) but also have contributions from electron impact excitation of  $\text{CO}$  (Bhardwaj & Raghuram 2011).  $\text{CO}_2$  production rates can be measured via high spectral resolution ground-based observations of  $\text{O}[I]$  when cometary and telluric emission is significantly separated by Doppler shift (McKay et al. 2012; Raghuram & Bhardwaj 2014; Decock et al. 2015), but this technique was not used on Chiron, Hale-Bopp or 29P. Using directly measured  $\text{CO}$  and  $\text{CO}_2$  production rates at approximately the same time from the literature, we calculate production rate ratios of  $Q(\text{CO}_2)/Q(\text{CO}) \sim 0.1\text{--}0.3$  for Hale-Bopp between 4–5 AU (Table 4). Searches for  $\text{CO}_2$  in 29P yielded upper limits of  $Q(\text{CO}_2)/Q(\text{CO}) \sim 0.01$  (Ootsubo et al. 2012; Reach et al. 2013a), roughly ten times lower than for Hale-Bopp at  $\sim 6$  AU. Clearly, at these large heliocentric distances,  $\text{CO}_2$  is not a significant driver for activity in either Hale-Bopp or 29P. Interestingly, the Hale-Bopp and 29P  $Q(\text{CO}_2)/Q(\text{CO})$  ratios are

significantly lower than what is reported for many other periodic or dynamically new comets Feldman et al. (1997b); A’Hearn et al. (2012); Bauer et al. (2015b); Reach et al. (2013b); Ootsubo et al. (2012). It is important to note that most of these measurements of other comets were obtained at heliocentric distances of 1 to 2.5 AU, which is much closer to the Sun than the CO<sub>2</sub> measurements in 29P and Hale-Bopp. It is possible that the production rate ratios of CO<sub>2</sub> and CO vary in distance from the Sun for an individual comet. The production rate ratios may not reflect the nucleus abundances, but rather the activity mechanism dominant at the time of observations. For example, at 29P’s distance from the Sun, the effective surface temperature (black-body) is roughly 120 K, which straddles the threshold for water ice amorphous-crystalline transition. Due to differences in volatility (sublimation pressures and rates), released CO will immediately flow outside, while released CO<sub>2</sub> would diffuse in the nucleus and may even re-condense at various depths. The presence of ice and clathrate reservoirs, for CO<sub>2</sub> and CO, could introduce alternative pathways. However, the location of these components will have to be very close to the surface, within  $\sim 1$  skin depth, in order to match the quiescent activity of 29P.

Indeed, the measured  $Q(\text{CO}_2)/Q(\text{CO})$  ratio increased as Hale-Bopp approached the Sun, which may be partly due to higher sublimation temperature for CO<sub>2</sub> (see Table 1) being reached by the comet. As part of a large infrared survey of comets that included 9 comets beyond 4 AU, Kelley et al. (2013) calculated each comet’s  $ef\rho$ , which is a quantity used to approximate the dust production rate. The study showed that  $\log Q(\text{CO}_2)/ef\rho$  broke into two groups of behavior for comets inside and outside 4 AU (see Figure 9 in Bauer et al. (2015b)). The authors of that survey suggest that within 4 AU, CO<sub>2</sub> activity may be endogenic with the dust. This may be attributable to different source regions (surface versus sub-surface) for cometary CO<sub>2</sub> and CO emissions. Further searches for CO and CO<sub>2</sub> emission from other distantly active comets are needed to test models of volatile production. Hale-Bopp and 29P appear to be CO-rich comets.

### 5.3. Spectral Line Profiles

Additional information is contained in spectral line profiles about how gas is emitted from a comet nucleus. For example, consider that the millimeter wavelength spectral line profiles of CO for Hale-Bopp (when beyond 4 AU), 29P and Chiron are all very narrow ( $< 0.5$  km/s), and sometimes are blue shifted by a small amount,  $\sim 0.3$ - $0.5$  km s $^{-1}$ . The numerical values of the velocity shifts are consistent with CO escaping from the nucleus at velocities corresponding to hydrodynamical escape for  $v \sim 0.4$  km s $^{-1}$  (Festou et al. 2001; Gunnarsson et al. 2003). The spectra’s blue-shifts indicate that the CO molecules’ velocity vector is primarily toward the Sun (and hence, the Earth, due to typically small phase angles), and the emission can be understood if it occurs on the sunward side of the nucleus. Such narrow lines indicate a narrow distribution of fluxes coming off the nucleus, which in turn probably indicates a singular source for the CO, at least in terms of the temperature and depth. There is a narrow range of thermal velocities that the CO molecules experience, once released, and there is a specific length scale that these molecules traverse before leaving the surface.

Sublimation from an icy grain halo is expected when an active comet is  $\sim 4$ - $6$  AU from the Sun. This occurred in Hale-Bopp’s coma at  $\sim 5$  AU from the Sun, and there is strong evidence that this develops in 29P and around other comets, such as Bowell, at 5 AU. This is the likely origin of most of the CH<sub>3</sub>OH, OH, HCN, H<sub>2</sub>CO and H<sub>2</sub>S emission in Hale-Bopp beyond 4 AU, as is illustrated in Figure 1. Interestingly, as Hale-Bopp moved closer to the Sun (from 5 to 4 AU) the linewidths of methanol increased from  $\sim 1$  to  $2$  km s $^{-1}$ , while the CO linewidths remained relatively constant, which further illustrates the differing behavior for CO and CH<sub>3</sub>OH at large heliocentric distances (Womack et al. 1997).

#### 5.4. A Consistent Set of CO Production Rates

Production rates for CO in these objects were published previously by several groups over 20 years with different models and assumptions, including Senay & Jewitt (1994); Crovisier et al. (1995); Womack et al. (1997); Womack & Stern (1999); Biver et al. (2002); Gunnarsson et al. (2003); Paganini et al. (2013); DiSanti et al. (1999). Differences in observing and modeling techniques make it difficult to assess similarities and differences of the production rates among the comets. In order to better compare the CO production, and probe the importance of nucleus size and thermal history, we derived the CO production rates using our own data for Hale-Bopp, 29P and Chiron in a consistent manner. The data for Hale-Bopp and Chiron were previously published using simpler models (Womack et al. 1997; Womack & Stern 1999). Most of the data for 29P are new and were obtained during 2016 Feb to May using the Arizona Radio Observatory 10-m Submillimeter Telescope (SMT)(Wierzbos et al., in preparation). The 29P CO data are part of a separate project and a full analysis will be published later. For now, we present the dates, heliocentric distances and derived production rates in Table 5. One additional data point for 29P was taken from Graham & Womack (1995). We assumed isotropic outgassing of CO from the nucleus, rotational and excitation temperatures of Biver et al. (2002) and expansion velocities from Gunnarsson et al. (2008). The excitation model includes both collisional and fluorescence excitation in a manner similar to Crovisier & Le Bourlot 1983 and Biver (1997). Applying a cone ejection model would reduce the numbers in Figure 2 by 40%, but would not otherwise change the results. In Figure 2, we plot the new CO production rates for Hale-Bopp, 29P and Chiron. The Hale-Bopp and 29P production rates are comparable to values derived by Gunnarsson et al. (2003, 2008). In Figure 2 we also include  $Q(\text{CO})$  values for Hale-Bopp taken from Gunnarsson et al. (2003), to extend the heliocentric range for Hale-Bopp; these values were not recalculated, because they used the same modeling parameters as our new model. The upper limit for Chiron was taken from Drahus et al.

(2016).

The Hale-Bopp CO production rates in Figure 2 are all pre-perihelion and follow the relationship  $Q(\text{CO}) = 3.5 \times 10^{29} r^{-2.2}$  molecules/second, where  $r$  is heliocentric distance in astronomical units (AU). This heliocentric dependence agrees with what was found by (Biver et al. 2002) for pre-perihelion data of Hale-Bopp. Later post-perihelion observations of the comet out to  $\sim 11$  AU showed that  $Q(\text{CO})$  followed a slightly less steep  $r^{-2}$  dependence (Biver et al. 2002; Gunnarsson et al. 2003). The pre-perihelion slope is steeper than one would expect for a mechanism driven solely by insolation, which would produce a  $r^{-2}$  dependence. The steeper slope may indicate that there is an additional source of energy in this regime, such as crystallization of water ice. Based on the discussion and analysis of Gunnarsson et al. (2003), we extrapolated the  $Q(\text{CO})$  relationship for Hale-Bopp out to 11 AU, assuming an  $r^{-2}$  dependence to indicate the likely CO production rates at larger heliocentric distances.

When adjusted for heliocentric distance, CO production rates in three distantly active comets are remarkably uniform, despite different thermal processing histories (long-period vs. Centaurs) and different nucleus sizes. We explore the apparently similar CO production rates in the next section.

### 5.5. Observational Constraints to Existing Models of Distant Activity

The models that best explain the quiescent activity of Hale-Bopp and 29P are similar. A porous comet nucleus comprising a mixture of ices and grains with a dust mantle at the surface best fits the data obtained so far (e.g., Enzian et al. 1997; Enzian 1999; Capria et al. 2002). In these models, crystallization of amorphous water ice near the surface and subsequent release of trapped CO molecules is the dominant cause of activity for 29P



and Hale-Bopp within 7 AU. Activity in Hale-Bopp beyond 8 AU is more likely caused by sublimation of near-surface CO ice, since the heating rate is too low for crystallization to proceed in any appreciable rate. The survival of near-surface CO ice may be aided by the low thermal conductivity maintained in very porous surface layers. Existing in-situ measurements of comet nuclei point to a highly-porous bulk, as for the Rosetta and Deep Impact measurements of comets 67P and 9P, respectively (Sierks et al. 2015, A’Hearn et al. 2005). However, a porosity gradient has been inferred for 67P (from the CONSERT sounding experiment), with an upper limit on near-surface porosity of 30. In any case there should exist a long-term reservoir for highly-volatile species, such as CO. The distinction between the effects of an amorphous/crystalline water ice phase and a gradient in layering and insulation falls outside the scope of this work and will be pursued by systematic modeling efforts.

Moreover, the CO emission in 29P and Hale-Bopp has sunward velocity shifts at large heliocentric distances. This implies that the CO released by both methods (sublimation of CO ice and release of trapped CO during the crystallization of water ice) occurs from the sub-solar regions of the nuclei. For Chiron, the surface temperatures are too warm for solid CO or CO<sub>2</sub> to be near the surface and sublimate, so instead, crystallization of water ice and release of trapped gases is the more likely model (Prialdnik et al. 1995; Capria et al. 2000). A high obliquity for the rotation axis would allow Chiron’s sub-solar regions to be heated enough by the Sun to reach the measured color temperatures, which is also high enough for crystallization to occur. These models also reproduce the quiescent dust production rates of the comets.

However, we note that recent spacecraft data have revealed how geologically diverse comets are. This surface geology and morphology evolution and the connection to the sub-surface layers are a function of both origin and evolution. Thus, it is not just the specific

diffusivity and conductivity of the icy and silicate components, but also the configurations, mixing ratios and dynamics of the different constituents that become important. Since comets are significantly porous (e.g., Patzold et al. 2016; A’Hearn et al. 2011, 2005), the way the porous medium evolves together with compositional and structural changes (phase transitions, gas flow, cavities, small impacts, out-gassing) affects the determination of bulk transport properties. Models of these interactions are inherently susceptible to some degeneracy in the choice of parameters. The more chemical and physical information we have about the nucleus and the behavior of the coma at various distances, the better we can constrain the modeled profiles and compositions.

Gaseous outbursts can be explained if a region unusually rich in CO ice sublimates when exposed to the Sun, or if a crystallization burst of water ice occurs. Either process will cause an increase in CO and dust production (if there is much dust in that region). Therefore, large dust jets emerge from cracks in the surface after being triggered by a gaseous outburst, while the bulk of the observed CO (that generates the quiescent activity) percolates through the comet surface that is at or near the sub-solar spot. Outbursts in 29P, in particular, are possibly triggered by surface erosion of the dust mantle (Enzian et al. 1997). For Chiron, sublimation of CO ice pockets is not likely, since, as discussed previously, the surface temperatures are too warm for CO ice to be present. Instead, amorphous water ice crystallization bursts are considered to be the most likely cause of outbursts for Chiron.

The mechanisms proposed to explain the distant activity in Hale-Bopp, 29P and Chiron are possible in any comet which contains amorphous ice with trapped CO gas, as well as frozen CO in their nuclei, as long as these materials are sufficiently near the surface to be heated to the crystallization and/or sublimation temperatures. One might wonder why most comets are not reported to be active until within 3 AU of the Sun. One possibility is that most short-period comets exhausted their reservoirs of CO (and other

supervolatile ice) and converted their amorphous ice to the crystalline phase many millions (or even billions) of years ago. Any remaining frozen CO and amorphous ice is too deeply buried to be heated above the crystallization and sublimation temperatures during their orbits. Another important point is that the nuclei of Hale-Bopp, 29P and Chiron are larger than those of most typical comets, and this is probably responsible for much of the distant activity. The larger volume exposes more material to heating, which provides more opportunities for sublimation and crystallization. Some smaller, long-period comets may exhibit CO production beyond 3 AU, but the quantities are too low to be detected with current equipment.

Orbital history is thought to play a role in devolatilizing comet nuclei. Hale-Bopp’s orbit places it in the long-period comet category, which means it has experienced few heating cycles over its lifetime, especially when compared to Chiron and 29P. It is dynamically young and has probably experienced very different perihelion/aphelion evolution than low-inclination bodies in the outer solar system (Bailey et al. 1996). As such, the reservoirs of volatile species in the nucleus have been processed in a different manner and could have remained more accessible to subsequent apparition. Large gas fluxes from previously untapped reservoirs of volatile species, which can efficiently entrain and drag dust grains from various depths in the nucleus, could have been the main source of the distinctive brightness of Hale-Bopp. The highly-volatile nature of the gas (and perhaps larger abundances of CO) may have been the main cause for very distant activity, both pre- and post-perihelion. 29P orbits much closer to the Sun, at  $r \sim 6$  AU, and thermal evolution from previous orbits probably depleted any highly-volatile solid ice from at least the first 100 or so meters. Accessible solid ice layers are probably rare, and thus not the main driver of activity for 29P. This is also probably true, to some extent, for Chiron, which orbits between 8.5 - 13 AU. By this measure alone, Hale-Bopp should have produced significantly more CO than 29P or Chiron. However, as Figure 2 shows, the CO production rates are

consistent between the comets. 29P produces CO at approximately the same rate as was observed in Hale-Bopp when it was at  $r \sim 6$  AU. Hale-Bopp’s and 29P’s very different orbital histories appear not to be reflected in their CO production rates at 6 AU. Chiron is a little more complicated to sort out. The CO emission detection in Chiron at 8.5 AU is consistent with the CO production rate in Hale-Bopp at about the same heliocentric distance post-perihelion. However, it is important to keep in mind that other searches for CO in Chiron led to upper limits which were significantly lower than the detection, which presumably occurred during an outburst. The non-detection limit made over two years implies that if Chiron does continually emit CO, it is likely at a much lower rate than Hale-Bopp or 29P. Dust production rates estimated from optical-infrared images are also consistent with significantly lower activity overall compared to Hale-Bopp at this distance (Romon-Martin et al. 2003; Weiler et al. 2003). Given the low dust production rates, Chiron is not likely to be outgassing significant amounts of another volatile, such as CO<sub>2</sub>. The Chiron data are consistent with very little constant volatile outgassing punctuated by sporadic outbursts.

Although Hale-Bopp’s long orbital period means that it is substantially less heated/processed than short-period comets, it has endured several passages near the Sun, which may be evident in comparisons with a true dynamically new comet, making its first perihelion approach. Detailed comparisons of observations of Hale-Bopp with such dynamically new comets at large distances would be very useful and should be encouraged. Currently, very few direct comparisons are possible beyond  $\sim 2$  AU, but one recently studied dynamically new comet, C/2009 P1 Garradd, showed a striking difference. Garradd did not show the strong correlation between CO activity and heliocentric distance as Hale-Bopp. Rather than show a symmetric increase and decrease of CO around perihelion, Garradd’s CO production continued to increase throughout the entire time period that could be studied, out to  $\sim 2$ -3 AU post-perihelion (Feaga et al. 2014; McKay et al. 2015).

Unfortunately, observations of CO emission beyond 4 AU do not exist for comet Garradd. It would be particularly valuable to compare CO behavior for these two classes of comets when they are beyond the water-ice sublimation limit. Also, closer to the Sun, CO may be produced in significant amounts as daughter products from parent species. Such competing sources for CO production near the Sun complicates efforts to account for how much CO is natal and driving the long-term activity.

Of the three objects discussed in this paper, two that have very different orbital histories (29P and Hale-Bopp) and thus should have very different CO production rates, in fact have very similar CO production rates. In addition, two which are classified as Centaurs with relatively close-in orbits (29P and Chiron) are expected to produce similar amounts of CO had they started with similar compositions. However, they have vastly different CO production rates. This is a very small sample set, obviously, but from studying these three objects we conclude that orbital history alone cannot explain the CO production rates in these objects. Further constraining measurements of CO emission from other Centaurs are needed to explore the role CO outgassing plays in Centaurs.

### **5.6. CO Output Adjusted For Nucleus Size**

A comet’s size is also expected to be correlated with how productive it is when it is heated by the Sun. For larger objects, once amorphous ice starts transitioning, triggered by small increases in temperature (from insolation, impacts, chemical reactions, etc.), it will depend only on the heat wave coming in from the surface. This heat wave is just a function of heliocentric distance, if we assume all other properties are similar (material, porosity, distribution, etc.).

Larger comets are more susceptible to radiogenic heating, which may lead to

devolatilization of the original ice. As discussed earlier, comets smaller than 10 km probably have their initial temperature preserved deeper than about 100 meters. However, 29P, Chiron and Hale-Bopp all have radii larger than 10 km, and so probably experienced some amount of radiogenic heating. Chiron is much larger than 29P and Hale-Bopp and so probably underwent even more radiogenic heating (unless 29P and Hale-Bopp are fragments of larger objects). Consequently, on the basis of size, one might expect Chiron to be more processed, and thus have less outgassing than 29P or Hale-Bopp. On the other hand, if one assumes comet nuclei to be roughly heterogeneous, then bigger comets should have higher outputs when heated.

CO emission was searched for, and not found, in a collection of KBO’s and Centaurs by Bockelée-Morvan et al. (2001); Jewitt et al. (2008); Drahus et al. (2016). Many of the Centaurs were first observed by Bockelée-Morvan et al. (2001) and Jewitt et al. (2008) and then re-analyzed by Drahus et al. (2016), who also made new observations. The authors of the first survey proposed that if the objects’ CO activity followed the trend of Hale-Bopp’s gas activity with heliocentric distance, and is proportional to the object’s diameter,  $D$ , then the relationship  $Q(\text{CO}) \sim r^{-2} \times D^2$  should hold, and CO should have been detected in these very distant objects. The upper limits they obtained are significantly below what would be predicted from this simple scaling law, which they conclude is evidence that these objects underwent significant CO devolatilization since their formation (De Sanctis et al. 2001b). The authors of the second survey drew the same conclusions about Centaurs likely being depleted in CO using similar arguments, whereas the third survey raised the question of whether CO outgassing should be correlated with heliocentric distance or size, but instead a small heliocentric distance might be more important. 29P is a notable exception to the list of apparently CO-depleted Centaurs, and its nearly circular orbit has a relatively small heliocentric distance of  $\sim 6$  AU.

To explore this further, we calculated CO “specific production rates,” which are the production rates divided by the square of the nucleus diameter. Specific production rates were calculated for Hale-Bopp, 29P and Chiron using CO production rates from Figure 2. Note that the Chiron upper limit at  $\sim 9.5$  AU is from Drahus et al. (2016), which they recalculated using Bockelée-Morvan et al. (2001) data. The specific production rates are plotted in Figure 4. Accordingly, Chiron is approximately 5-15 times depleted in CO when compared to Hale-Bopp, a proxy for a relatively unprocessed comet.<sup>4</sup> We do not have our own Hale-Bopp data at 8-10 AU, and hence we extrapolated  $Q(\text{CO})$  from the  $r^{-2}$  fit to the  $Q(\text{CO})$  data, which is also consistent with  $Q(\text{CO})$  values from Gunnarsson et al. (2003). We conclude that there is measurably less CO produced per surface area from Chiron than either Hale-Bopp or 29P. This is consistent with radiogenic heating devolatilization being an important parameter in nucleus modeling, since Chiron is much larger than either of the other two comets.

As discussed in the previous section, Hale-Bopp and 29P have very similar CO production rates, even when corrected for nucleus size. We see no evidence for devolatilization for 29P when compared to Hale-Bopp; in fact, when outbursting, 29P outproduces Hale-Bopp by almost a factor of ten. This may point to 29P being a more recent entrant to the inner solar system than Chiron.

Since Chiron does not get closer than  $\sim 8.5$  AU, where  $T_{bb} \sim 100\text{K}$ , it can maintain a

---

<sup>4</sup>A similar calculation was performed by Bockelée-Morvan et al. (2001) and found Chiron to be depleted by a factor of  $\sim 35$  with respect to Hale-Bopp. This difference in depletion values can be largely explained by different values used for Hale-Bopp’s nucleus diameter,  $D$ , and CO production rate at 8-9 AU. For example, Bockelée-Morvan et al. (2001) assumed  $D=40$  km diameter (we use 60 km) and they used an older CO production rate value for Hale-Bopp that was later updated by Gunnarsson et al. (2003), which we also use.

slow crystallization rate of  $\sim 1000$  years (and rate of trapped volatile release), if we assume maximum efficiency. Perhaps Chiron never experienced large temperature excursions to its surface, since the perihelion was never much inside of its current one. However, by considering the noted higher color temperature and low CO production rate, we find it consistent with Chiron’s being appreciably devolatilized over a fresher object like Hale-Bopp. Also, Chiron’s interior may be warmer due to early radiogenic heating and slow cooling rates, as it is a larger object than both Hale-Bopp and 29P.

## 6. Conclusions

All Hale-Bopp, 29P and Chiron have in common that: 1) They exhibit long-term quiescent activity beyond 4 AU that is punctuated by sporadic outbursts; 2) Emission from CN and CO was seen in their coma; 3) The CO line profiles were narrow,  $\Delta v(\text{FWHM}) \sim 0.3\text{-}0.5 \text{ km s}^{-1}$ ; 4) They have spent most of their lifetime far from the Sun;<sup>5</sup> 5) They have larger-than-usual nuclei.

There are notable differences among the comets, including: 1) The CO emission had blue-shifted velocity components of  $\sim -0.4 \text{ km/s}$  (sunward) for 29P and Hale-Bopp, but almost no shift for Chiron’s emission; 2) CO was seen only once in Chiron, but was repeatedly observable for long-term study in Hale-Bopp and 29P (and 29P is observable, even now); 3) Hale-Bopp had much higher dust production rates than seen in 29P or Chiron.

Sublimation or escape of molecules from a grain halo at  $\sim 5\text{-}6 \text{ AU}$  appears to be a

---

<sup>5</sup>Chiron and 29P have only recently entered their current orbits and may be precursors to Jupiter Family comets (Fernandez & Gallardo 1994), and Hale-Bopp has an aphelion of  $\sim 360 \text{ AU}$ , spends most of its time at very large heliocentric distances.



typical development in distantly active comets, and may be the main source of emission of OH, HCN, CH<sub>3</sub>OH, H<sub>2</sub>CO, and H<sub>2</sub>S in Hale-Bopp between 3 – 6 AU. This may also explain the origin of OH and CN molecules in other distant comets. Spectral line profiles and spatial mapping should be used whenever possible to determine a nuclear or extended origin for volatiles in distant comets. Observed radio line profiles are consistent with the development and sublimation of icy grains in the coma at about 5-6 AU, and this is probably a common feature in distantly active comets, and an important source of other volatiles within 5 AU. Note that narrow CO line profiles for all three main bodies in this study indicate a nuclear origin for CO beyond  $\sim 4$  AU, and not an extended source, as with these other molecular cases.

Our calculated CN/CO and CO<sub>2</sub>/CO production rate ratios for Hale-Bopp and 29P show that HCN and CO<sub>2</sub> were both produced in significantly smaller amounts than CO, and can only be minor contributors to distant activity of these two objects. For Chiron, no limits exist for CO<sub>2</sub> emission, and CN and CO were both detected only once at the  $\sim 3.5\sigma$  level. The CN measurements are consistent with HCN being an insignificant contributor to Chiron’s coma. The CO data correspond to a gas production rate high enough to drive the observed dust coma activity; however, the CO detected may have also resulted from an outburst and we cannot rule out significant contributions from undetected CO<sub>2</sub> or other supervolatile gases. We point out that the CN/CO production rate ratios that we derive from the literature are remarkably similar in all three distantly active comets, which warrants follow-up study.

When adjusted for heliocentric distance, our analysis shows that CO production rates in three distantly active comets are remarkably uniform, despite different thermal processing histories (long-period vs. Centaurs) and different nucleus sizes. Specific CO production rates,  $Q(\text{CO})/D^2$ , were calculated in order to take into account nucleus size,

which is predicted to play a large role in cometary activity. We find that orbital history does not appear to play a significant role in explaining the CO production rates for 29P and Hale-Bopp, which confirms the conclusion in A’Hearn et al. (2012) for comets within 2 AU. 29P outproduces Hale-Bopp at the same heliocentric distance, although it has been subjected to solar heating far longer, and models predict it should have been devolatilized over a fresher comet, like Hale-Bopp. However, we may see evidence for the relevance of nucleus size when considering specific production rates. If CO is present in Chiron’s coma on a long-term basis, it must be in relatively small amounts and consistent with a CO depletion by at least 5-15 times over Hale-Bopp, perhaps due to increased radiogenic heating made possible by its much larger size or its higher processing due to orbital history.

The model which best reproduces the distant activity of 29P and Hale-Bopp is a comet nucleus composed of dust, amorphous water ice and smaller amounts of trapped CO and CO<sub>2</sub> trapped in the amorphous ice and a build-up of a thin porous dust mantle (Priyalnik 1997a,b). Within  $\sim 4 - 7$  AU, the water ice undergoes crystallization near the surface and releases trapped gases and dust. There is a large range of free parameters in the models. The spin state and specific porous medium properties play a large role in the differences in activity between comets. The release of CO and subsequent permeability of the gas flow could inhibit emission, especially if the local temperature (and pressure) gradients vary. This variation could be a strong function of solar radiation heating and surface cooling, which are functions of the spin state and surface morphology. Since Rosetta, the latter has become an increasingly important factor (Thomas et al. 2015).

Models for Chiron’s distant activity are presented in Priyalnik et al. (1995); Capria et al. (2000); Fanale & Salvail (1997). The first two include amorphous ice and rely on release of trapped CO, while the latter starts with a layered model of dust mantle, thick water ice layer and CO layer underneath. The amorphous ice models better reproduce the distant activity,

although they are constrained by a lack of observations of CO and dust production. The latter is a convolution of gas fluxes, dust properties and coma behavior. Models dominated by crystalline water ice and CO/CO<sub>2</sub> ices are not successful (Prialdnik et al. 1995). Instead, Chiron’s activity appears to be best explained by a release of trapped volatile species in the water ice matrix. However, a more complete understanding of the outburst or quiescent nature of this activity would require more measurements of CO production rates, at different times. An optimal addition would be observations of other species (e.g., methanol, methane, CO<sub>2</sub>, etc.), which would enable more stringent constraints on the nucleus’ composition ratios and thermal history. Radiogenic heating may be important for explaining Chiron’s low-level activity that appears CO-depleted. Furthermore, if rings are confirmed around Chiron, then previously reported long-term changes in visual magnitude and infrared spectral ice features should be re-examined.

## 7. Acknowledgements

The authors thank the anonymous referee for useful comments and feedback, which improved the paper. This material is based upon work supported by (while MW was serving at) the National Science Foundation (NSF). MW also acknowledges support from NSF grants AST-1009933 and AST-1615917. Any opinion, findings, and conclusions or recommendations expressed in this material are those of the author(s) and do not necessarily reflect the views of the National Science Foundation. The SMT is operated by the Arizona Radio Observatory (ARO), the Steward Observatory, and the University of Arizona, with support through the NSF University Radio Observatories program (AST-1140030).

## REFERENCES

- A’Hearn, M. F., Belton, M. J. S., Delamere, W. A., Feaga, L. M., Hampton, D., Kissel, J., Klaasen, K. P., McFadden, L. A., Meech, K. J., Melosh, H. J., Schultz, P. H., Sunshine, J. M., Thomas, P. C., Veverka, J., Wellnitz, D. D., Yeomans, D. K., Besse, S., Bodewits, D., Bowling, T. J., Carcich, B. T., Collins, S. M., Farnham, T. L., Groussin, O., Hermalyn, B., Kelley, M. S., Kelley, M. S., Li, J.-Y., Lindler, D. J., Lisse, C. M., McLaughlin, S. A., Merlin, F., Protopapa, S., Richardson, J. E., & Williams, J. L. 2011, *Science*, 332, 1396
- A’Hearn, M. F., Belton, M. J. S., Delamere, W. A., Kissel, J., Klaasen, K. P., McFadden, L. A., Meech, K. J., Melosh, H. J., Schultz, P. H., Sunshine, J. M., Thomas, P. C., Veverka, J., Yeomans, D. K., Baca, M. W., Busko, I., Crockett, C. J., Collins, S. M., Desnoyer, M., Eberhardy, C. A., Ernst, C. M., Farnham, T. L., Feaga, L., Groussin, O., Hampton, D., Ipatov, S. I., Li, J.-Y., Lindler, D., Lisse, C. M., Mastrodemos, N., Owen, W. M., Richardson, J. E., Wellnitz, D. D., & White, R. L. 2005, *Science*, 310, 258
- A’Hearn, M. F., Feaga, L. M., Keller, H. U., Kawakita, H., Hampton, D. L., Kissel, J., Klaasen, K. P., McFadden, L. A., Meech, K. J., Schultz, P. H., Sunshine, J. M., Thomas, P. C., Veverka, J., Yeomans, D. K., Besse, S., Bodewits, D., Farnham, T. L., Groussin, O., Kelley, M. S., Lisse, C. M., Merlin, F., Protopapa, S., & Wellnitz, D. D. 2012, *ApJ*, 758, 29
- A’Hearn, M. F., Millis, R. C., Schleicher, D. O., Osip, D. J., & Birch, P. V. 1995, *Icarus*, 118, 223
- A’Hearn, M. F., Schleicher, D. G., Millis, R. L., Feldman, P. D., & Thompson, D. T. 1984, *AJ*, 89, 579

- Bar-Nun, A., Kleinfeld, I., & Kochavi, E. 1988, *Phys. Rev. B*, 38, 7749
- Bar-Nun, A. & Owen, T. 1998, in *Astrophysics and Space Science Library*, Vol. 227, *Solar System Ices*, ed. B. Schmitt, C. de Bergh, & M. Festou, 353
- Bauer, J. M., Stevenson, R., Kramer, E., Mainzer, A. K., Grav, T., Masiero, J. R., Fernández, Y. R., Cutri, R. M., Dailey, J. W., Masci, F. J., Meech, K. J., Walker, R., Lisse, C. M., Weissman, P. R., Nugent, C. R., Sonnett, S., Blair, N., Lucas, A., McMillan, R. S., Wright, E. L., WISE, t., & NEOWISE Teams. 2015a, *ApJ*, 814, 85
- . 2015b, *ApJ*, 814, 85
- Belton, M. J. S. & Melosh, J. 2009, *Icarus*, 200, 280
- Bhardwaj, A. & Raghuram, S. 2011, *MNRAS*, 412, L25
- Biver. 1997, *Universit Paris 7*
- Biver, N., Bockelee-Morvan, D., Colom, P., Crovisier, J., Davies, J. K., Dent, W. R. F., Despois, D., Gerard, E., Lellouch, E., Rauer, H., Moreno, R., & Paubert, G. 1997a, *Science*, 275, 1915
- Biver, N., Bockelée-Morvan, D., Colom, P., Crovisier, J., Germain, B., Lellouch, E., Davies, J. K., Dent, W. R. F., Moreno, R., Paubert, G., Wink, J., Despois, D., Lis, D. C., Mehringer, D., Benford, D., Gardner, M., Phillips, T. G., Gunnarsson, M., Rickman, H., Winnberg, A., Bergman, P., Johansson, L. E. B., & Rauer, H. 1997b, *Earth Moon and Planets*, 78, 5
- Biver, N., Bockelée-Morvan, D., Colom, P., Crovisier, J., Henry, F., Lellouch, E., Winnberg, A., Johansson, L. E. B., Gunnarsson, M., Rickman, H., Rantakyö, F., Davies, J. K., Dent, W. R. F., Paubert, G., Moreno, R., Wink, J., Despois, D., Benford, D. J.,

- Gardner, M., Lis, D. C., Mehringer, D., Phillips, T. G., & Rauer, H. 2002, *Earth Moon and Planets*, 90, 5
- Biver, N., Bockelée-Morvan, D., Crovisier, J., Davies, J. K., Matthews, H. E., Wink, J. E., Rauer, H., Colom, P., Dent, W. R. F., Despois, D., Moreno, R., Paubert, G., Jewitt, D., & Senay, M. 1999, *AJ*, 118, 1850
- Biver, N., Rauer, H., Despois, D., Moreno, R., Paubert, G., Bockelée-Morvan, D., Colom, P., Crovisier, J., Gérard, E., & Jorda, L. 1996, *Nature*, 380, 137
- Bockelee-Morvan, D., Biver, N., Crovisier, J., de Val-Borro, M., Fulton, T., Hartogh, P., Hutsemékers, D., Jarchow, C., Jehin, E., Kidger, M., Kueppers, M., Lellouch, E., Lis, D., Manfroid, J., Moreno, R., Rengel, M., Swinyard, B. C., Szutowicz, S., Vandenbussche, B., & HssO Team. 2010, in *Bulletin of the American Astronomical Society*, Vol. 42, AAS/Division for Planetary Sciences Meeting Abstracts #42, 946
- Bockelée-Morvan, D., Biver, N., Jehin, E., Cochran, A. L., Wiesemeyer, H., Manfroid, J., Hutsemékers, D., Arpigny, C., Boissier, J., Cochran, W., Colom, P., Crovisier, J., Milutinovic, N., Moreno, R., Prochaska, J. X., Ramirez, I., Schulz, R., & Zucconi, J.-M. 2008, *ApJ*, 679, L49
- Bockelee-Morvan, D., Biver, N., Opitom, C., Hutsemekers, D., Crovisier, J., Jehin, E., Hartogh, P., Szutowicz, S., Lellouch, E., Kidger, M., Vandenbussche, B., Zakharov, V., & HSSO Team. 2014, in *Asteroids, Comets, Meteors 2014*, ed. K. Muinonen, A. Penttilä, M. Granvik, A. Virkki, G. Fedorets, O. Wilkman, & T. Kohout
- Bockelée-Morvan, D., Lellouch, E., Biver, N., Paubert, G., Bauer, J., Colom, P., & Lis, D. C. 2001, *Astron. and Astrophys.*, 377, 343
- Boehnhardt, H., Birkle, K., Fiedler, A., Jorda, L., Thomas, N., Peschke, S., Rauer, H.,

- Schulz, R., Schwehm, G., Tozzi, G., & West, R. 1997, *Earth Moon and Planets*, 78, 179
- Boice, D. C. & Huebner, W. F. 1993, in *Bulletin of the American Astronomical Society*, Vol. 25, AAS/Division for Planetary Sciences Meeting Abstracts #25, 1064
- Boss, A. P. 1994, *Icarus*, 107, 422
- Braunstein, M., Comstock, R., Hoffman, P., Womack, M., Deglman, F., Pinnick, D., Aaker, G., Goldschen, M., Jacobson, A., Zilka, J., Faith, D., Moore, S., Ricotta, J., Weist, A., & Modi, C. 1997, *Earth Moon and Planets*, 78, 219
- Brown, G. N. & Ziegler, W. T. 1979, *Adv. Cryogen. Engineering*, 25, 662
- Buratti, B. J. & Dunbar, R. S. 1991, *ApJ*, 366, L47
- Bus, S. J., A’Hearn, M. F., Schleicher, D. G., & Bowell, E. 1991, *Science*, 251, 774
- Bus, S. J., Bowell, E., Harris, A. W., & Hewitt, A. V. 1989, *Icarus*, 77, 223
- Bus, S. J., Buie, M. W., Schleicher, D. G., Hubbard, W. B., Marcialis, R. L., Hill, R., Wasserman, L. H., Spencer, J. R., Millis, R. L., Franz, O. G., Bosh, A. S., Dunham, E. W., Ford, C. H., Young, J. W., Elliott, J. L., Meserole, R., Olkin, C. B., McDonald, S. W., Foust, J. A., Sopata, L. M., & Bandyopadhyay, R. M. 1996, *Icarus*, 123, 478
- Bus, S. J., Stern, S. A., & A’Hearn, M. F. 1993, *Proceedings of the Distant Comet Activity Workshop*, 41
- Campins, H., Telesco, C. M., Osip, D. J., Rieke, G. H., Rieke, M. J., & Schulz, B. 1994, *AJ*, 108, 2318
- Capria, M. T., Coradini, A., & de Sanctis, M. C. 2002, *Earth Moon and Planets*, 90, 217

- Capria, M. T., Coradini, A., De Sanctis, M. C., & Orosei, R. 2000, *AJ*, 119, 3112
- Cochran, A. L. 2002, *ApJ*, 576, L165
- Cochran, A. L., Barker, E. S., & Cochran, W. D. 1980, *Astron. J.*, 85, 474
- Cochran, A. L. & Cochran, W. D. 1991, *Icarus*, 90, 172
- Cochran, A. L., Cochran, W. D., & Barker, E. S. 1982, *ApJ*, 254, 816
- . 2000, *Icarus*, 146, 583
- Cook, J. C., Desch, S. J., & Wyckoff, S. 2005, in *Bulletin of the American Astronomical Society*, Vol. 37, AAS/Division for Planetary Sciences Meeting Abstracts #37, 645
- Crifo, J. F., Rodionov, A. V., & Bockelée-Morvan, D. 1999, *Icarus*, 138, 85
- Crovisier, J. 1997, *Earth Moon and Planets*, 79, 125
- Crovisier, J., Biver, N., Bockelee-Morvan, D., Colom, P., Jorda, L., Lellouch, E., Paubert, G., & Despois, D. 1995, *Icarus*, 115, 213
- Crovisier, J. & Le Bourlot, J. 1983, *A&A*, 123, 61
- Crovisier, J., Leech, K., Bockelée-Morvan, D., Brooke, T. Y., Hanner, M. S., Altieri, B., Keller, H. U., & Lellouch, E. 1997, in *ESA Special Publication*, Vol. 419, *The first ISO workshop on Analytical Spectroscopy*, ed. A. M. Heras, K. Leech, N. R. Trams, & M. Perry, 137
- De Sanctis, M. C., Capria, M. T., & Coradini, A. 2001a, *AJ*, 121, 2792
- . 2001b, *AJ*, 121, 2792
- Decock, A., Jehin, E., Rousselot, P., Hutsemékers, D., Manfroid, J., Raghuram, S., Bhardwaj, A., & Hubert, B. 2015, *A&A*, 573, A1



- Dello Russo, N., Kawakita, H., Vervack, R. J., & Weaver, H. A. 2016, *Icarus*, 278, 301
- Delsemme, A. H. & Miller, D. C. 1971, *Planet. Space Sci.*, 19, 1229
- Despois, D., Biver, N., Bockelée-Morvan, D., & Crovisier, J. 2005, in *IAU Symposium*, Vol. 231, *Astrochemistry: Recent Successes and Current Challenges*, ed. D. C. Lis, G. A. Blake, & E. Herbst, 469–478
- DiSanti, M., Mumma, N. J., Dello Russo, N., Magee-Sauer, K., Novak, R., & Rettig, T. W. 1999, *Nature*, 399, 662
- Dones, L., Brasser, R., Kaib, N., & Rickman, H. 2015, *Space Sci. Rev.*, 197, 191
- Drahus, M., Yang, B., Lis, D. C., & Jewitt, D. 2016, *MNRAS*
- Duffard, R., Lazzaro, D., Pinto, S., Carvano, J., Angeli, C., Alvarez-Candal, A., & Fernández, S. 2002, *Icarus*, 160, 44
- Duffard, R., Pinilla-Alonso, N., Ortiz, J. L., Alvarez-Candal, A., Sicardy, B., Santos-Sanz, P., Morales, N., Colazo, C., Fernández-Valenzuela, E., & Braga-Ribas, F. 2014, *A&A*, 568, A79
- Durda, D. D. & Stern, S. A. 2000, *Icarus*, 145, 220
- Elliot, J. L., Olkin, C. B., Dunham, E. W., Ford, C. H., Gilmore, D. K., Kurtz, D., Lazzaro, D., Rank, D. M., Temi, P., Bandyopadhyay, R. M., Barroso, J., Barucci, A., Bosh, A. S., Buie, M. W., Bus, S. J., Dahn, C. C., Foryta, D. W., Hubbard, W. B., Lopes, D. F., Marcialis, R. L., McDonald, S. W., Millis, R. L., Reitsema, H., Schleicher, D. G., Sicardy, B., Stone, R. P. S., & Wasserman, L. H. 1995, *Nature*, 373, 46
- Enzian, A. 1999, *Space Sci. Rev.*, 90, 131
- Enzian, A., Cabot, H., & Klinger, J. 1997, *A&A*, 319, 995

- Fanale, F. P. & Salvail, J. R. 1997, *Icarus*, 125, 397
- Farinella, P. & Davis, D. R. 1996, *Science*, 273, 938
- Feaga, L. M., A’Hearn, M. F., Farnham, T. L., Bodewits, D., Sunshine, J. M., Gersch, A. M., Protopapa, S., Yang, B., Drahus, M., & Schleicher, D. G. 2014, *AJ*, 147, 24
- Feldman, P. D., Cochran, A. L., & Combi, M. R. Spectroscopic investigations of fragment species in the coma, ed. M. C. Festou, H. U. Keller, & H. A. Weaver, 425–447
- Feldman, P. D., Festou, M. C., Tozzi, P., & Weaver, H. A. 1997a, *ApJ*, 475, 829
- . 1997b, *ApJ*, 475, 829
- Feldman, P. D., McPhate, J. B., Weaver, H. A., Tozzi, G.-P., & A’Hearn, M. F. 1996, in *Bulletin of the American Astronomical Society*, Vol. 28, AAS/Division for Planetary Sciences Meeting Abstracts #28, 1084
- Fernandez, J. A. 1980, *Icarus*, 42, 406
- Fernandez, J. A. & Gallardo, T. 1994, *A&A*, 281, 911
- Fernández, Y. R. 2000, *Earth Moon and Planets*, 89, 3
- . 2009, *Planet. Space Sci.*, 57, 1218
- Fernández, Y. R., Wellnitz, D. D., Buie, M. W., Dunham, E. W., Millis, R. L., Nye, R. A., Stansberry, J. A., Wasserman, L. H., A’Hearn, M. F., Lisse, C. M., Golden, M. E., Person, M. J., Howell, R. R., Marcialis, R. L., & Spitale, J. N. 1999, *Icarus*, 140, 205
- Festou, M. C., Barale, O., Davidge, T., Stern, S. A., Tozzi, G. P., Womack, M., & Zucconi, J. M. 1998, in *Bulletin of the American Astronomical Society*, Vol. 30, AAS/Division for Planetary Sciences Meeting Abstracts #30, 1089

- Festou, M. C., Gunnarsson, M., Rickman, H., Winnberg, A., & Tancredi, G. 2001, *Icarus*, 150, 140
- Fitzsimmons, A. & Cartwright, I. M. 1996, *MNRAS*, 278, L37
- Fornasier, S., Lellouch, E., Müller, T., Santos-Sanz, P., Panuzzo, P., Kiss, C., Lim, T., Mommert, M., Bockelée-Morvan, D., Vilenius, E., Stansberry, J., Tozzi, G. P., Mottola, S., Delsanti, A., Crovisier, J., Duffard, R., Henry, F., Lacerda, P., Barucci, A., & Gicquel, A. 2013, *A&A*, 555, A15
- Foster, M. J., Green, S. F., McBride, N., & Davies, J. K. 1999, *Icarus*, 141, 408
- Fox, J. L. & Black, J. H. 1989, *Geophys. Res. Lett.*, 16, 291
- Fray, N., Bénilan, Y., Cottin, H., Gazeau, M.-C., & Crovisier, J. 2005, *Planet. Space Sci.*, 53, 1243
- Fulle, M. 1992, *Nature*, 359, 42
- . 1994, *A&A*, 282, 980
- Ghormley, J. A. 1968, *J. Chem. Phys.*, 48, 503
- Graham, Jr., R. A. & Womack, M. 1995, in *B.A.A.S.*, Vol. 27, #186, 857
- Gronkowski, P. & Smela, J. 1998, *A&A*, 338, 761
- Groussin, O., Lamy, P., & Jorda, L. 2004, *A&A*, 413, 1163
- Gunnarsson, M., Bockelée-Morvan, D., Biver, N., Crovisier, J., & Rickman, H. 2008, *Astron. and Astroph.*, 484, 537
- Gunnarsson, M., Bockelée-Morvan, D., Winnberg, A., Rickman, H., Crovisier, J., Biver, N., Colom, P., Davies, J. K., Despois, D., Henry, F., Johansson, L. E. B., Moreno, R., Paubert, G., & Rantakyö, F. T. 2003, *A&A*, 402, 383

- Gunnarsson, M., Rickman, H., Festou, M. C., Winnberg, A., & Tancredi, G. 2002, *Icarus*, 157, 309
- Hahn, G. & Bailey, M. E. 1990, *Nature*, 348, 132
- Hanner, M. S. 1981, *Icarus*, 47, 342
- . 1984, *ApJ*, 277, L75
- Hartmann, W. K., Tholen, D. J., Meech, K. J., & Cruikshank, D. P. 1990, *Icarus*, 83, 1
- Haruyama, J., Yamamoto, T., Mizutani, H., & Greenberg, J. M. 1993, *J. Geophys. Res.*, 98, 15
- Hässig, M., Altwegg, K., Balsiger, H., Bar-Nun, A., Berthelier, J. J., Bieler, A., Bochsler, P., Briois, C., Calmonte, U., Combi, M., De Keyser, J., Eberhardt, P., Fiethe, B., Fuselier, S. A., Galand, M., Gasc, S., Gombosi, T. I., Hansen, K. C., Jäckel, A., Keller, H. U., Kopp, E., Korth, A., Kührt, E., Le Roy, L., Mall, U., Marty, B., Mousis, O., Neefs, E., Owen, T., Rème, H., Rubin, M., Sémon, T., Tornow, C., Tzou, C.-Y., Waite, J. H., & Wurz, P. 2015, *Science*, 347, aaa0276
- Hughes, D. W. 1991, in *Astrophysics and Space Science Library*, Vol. 167, IAU Colloq. 116: Comets in the post-Halley era, ed. R. L. Newburn, Jr., M. Neugebauer, & J. Rahe, 825–851
- Iro, N., Gautier, D., Hersant, F., Bockelée-Morvan, D., & Lunine, J. I. 2003, *Icarus*, 161, 511
- Irvine, W. M., Schloerb, F. P., Crovisier, J., Fegley, Jr., B., & Mumma, M. J. 2000, *Protostars and Planets IV*, 1159
- Ivanova, A., Afanasiev, V., Korsun, P., Baransky, A., Andreev, M., & Ponomarenko, V. 2015, *Highlights of Astronomy*, 16, 176

- Ivanova, O. V., Luk'yanyk, I. V., Kiselev, N. N., Afanasiev, V. L., Picazzio, E., Cavichia, O., de Almeida, A. A., & Andrievsky, S. M. 2016, *Planet. Space Sci.*, 121, 10
- Jewitt, D. 1990, *Astroph. J.*, 351, 277
- . 1993, *Proceedings of the Workshop on the Activity of Distant Comets*, 64
- Jewitt, D., Garland, C. A., & Aussel, H. 2008, *AJ*, 135, 400
- Jewitt, D., Senay, M., & Matthews, H. 1996, *Science*, 271, 1110
- Kelley, M. S., Lindler, D. J., Bodewits, D., A'Hearn, M. F., Lisse, C. M., Kolokolova, L., Kissel, J., & Hermalyn, B. 2013, *Icarus*, 222, 634
- Klinger, J. 1980, *Science*, 209, 634
- . 1981, *Icarus*, 47, 320
- Kouchi, A., Greenberg, J. M., Yamamoto, T., & Mukai, T. 1992, *ApJ*, 388, L73
- Kouchi, A. & Sirono, S.-i. 2001, *Geophys. Res. Lett.*, 28, 827
- Kouchi, A., Yamamoto, T., Kozasa, T., Kuroda, T., & Greenberg, J. M. 1994, *A&A*, 290
- Kulyk, I., Korsun, P., Rousselot, P., Afanasiev, V., & Ivanova, O. 2016, *Icarus*, 271, 314
- Lamy, P. L. 1974, *A&A*, 35, 197
- Larson, S. M. 1980, *ApJ*, 238, L47
- Laufer, D., Kochavi, E., & Bar-Nun, A. 1987, *Phys. Rev. B*, 36, 9219
- Lazzaro, D., Florczak, M. A., Angeli, C. A., Carvano, J. M., Betzler, A. S., Casati, A. A., Barucci, M. A., Doressoundiram, A., & Lazzarin, M. 1997, *Planet. Space Sci.*, 45, 1607

- Lebofsky, L. A., Tholen, D. J., Rieke, G. H., & Lebofsky, M. J. 1984, *Icarus*, 60, 532
- Lellouch, E., Crovisier, J., Lim, T., Bockelee-Morvan, D., Leech, K., Hanner, M. S., Altieri, B., Schmitt, B., Trotta, F., & Keller, H. U. 1998, *A&A*, 339, L9
- Levison, H. F. & Duncan, M. J. 1994, *Icarus*, 108, 18
- Lutz, B. L., Womack, M., & Wagner, R. M. 1993, *ApJ*, 407, 402
- Luu, J. X. & Jewitt, D. C. 1990, *AJ*, 100, 913
- Luu, J. X., Jewitt, D. C., & Trujillo, C. 2000, *ApJ*, 531, L151
- Magnani, L. & A’Hearn, M. F. 1986, *ApJ*, 302, 477
- Marcialis, R. L. & Buratti, B. J. 1993, *Icarus*, 104, 234
- Matthews, C. 1995, in *Astronomical Society of the Pacific Conference Series*, Vol. 74, *Progress in the Search for Extraterrestrial Life.*, ed. G. S. Shostak, 95
- Mazzotta Epifani, E., Palumbo, P., Capria, M. T., Cremonese, G., Fulle, M., & Colangeli, L. 2007, *MNRAS*, 381, 713
- McKay, A. J., Chanover, N. J., Morgenthaler, J. P., Cochran, A. L., Harris, W. M., & Russo, N. D. 2012, *Icarus*, 220, 277
- McKay, A. J., Cochran, A. L., DiSanti, M. A., Villanueva, G., Russo, N. D., Vervack, R. J., Morgenthaler, J. P., Harris, W. M., & Chanover, N. J. 2015, *Icarus*, 250, 504
- Meech, K. J. & Belton, M. J. S. 1990, *Astron. J.*, 100, 1323
- Meech, K. J., Belton, M. J. S., Mueller, B. E. A., Dicksion, M. W., & Li, H. R. 1993, *AJ*, 106, 1222
- Meech, K. J. & Jewitt, D. 1987, *Nature*, 328, 506

- Miles, R. 2016, *Icarus*, 272, 356
- Moreno, F. 2009, *ApJS*, 183, 33
- Mumma, M. J., Weissman, P. R., & Stern, S. A. 1993, in *Protostars and Planets III*, ed. E. H. Levy & J. I. Lunine, 1177–1252
- Ootsubo, T., Kawakita, H., Hamada, S., Kobayashi, H., Yamaguchi, M., Usui, F., Nakagawa, T., Ueno, M., Ishiguro, M., Sekiguchi, T., Watanabe, J.-i., Sakon, I., Shimonishi, T., & Onaka, T. 2012, *ApJ*, 752, 15
- Ortiz, J. L., Duffard, R., Pinilla-Alonso, N., Alvarez-Candal, A., Santos-Sanz, P., Morales, N., Fernández-Valenzuela, E., Licandro, J., Campo Bagatin, A., & Thirouin, A. 2015, *A&A*, 576, A18
- Paganini, L., Mumma, M. J., Boehnhardt, H., DiSanti, M. A., Villanueva, G. L., Bonev, B. P., Lippi, M., Käuff, H. U., & Blake, G. A. 2013, *Astroph. J.*, 766, 100
- Parker, J. W., Stern, S. A., Festou, M. C., A’Hearn, M. F., & Weintraub, D. 1997, *AJ*, 113, 1899
- Patashnick, H. 1974, *Nature*, 250, 313
- Patzold, M., Andert, T., Hahn, M., Asmar, S. W., Barriot, J.-P., Bird, M. K., Häusler, B., Peter, K., Tellmann, S., Grün, E., Weissman, P. R., Sierks, H., Jorda, L., Gaskell, R., Preusker, F., & Scholten, F. 2016, *Nature*, 530, 63
- Pierce, D. M. & A’Hearn, M. F. 2010, *ApJ*, 718, 340
- Prialnik, D. 1997a, *ApJ*, 478, L107
- . 1997b, *Earth Moon and Planets*, 77, 223

- Prialnik, D. & Bar-Nun, A. 1990a, *ApJ*, 363, 274
- . 1990b, *ApJ*, 363, 274
- Prialnik, D., Bar-Nun, A., & Podolak, M. 1987, *ApJ*, 319, 993
- Prialnik, D., Benkhoff, J., & Podolak, M. Modeling the structure and activity of comet nuclei, ed. G. W. Kronk, 359–387
- Prialnik, D., Brosch, N., & Ianovici, D. 1995, *MNRAS*, 276, 1148
- Prialnik, D., Egozi, U., Bar-Nun, A., Podolak, M., & Mekler, Y. 1992, in *Bulletin of the American Astronomical Society*, Vol. 24, AAS/Division for Planetary Sciences Meeting Abstracts #24, 1019
- Prialnik, D. & Podolak, M. 1995, *Icarus*, 117, 420
- . 1999, *Space Sci. Rev.*, 90, 169
- Prialnik, D., Sarid, G., Rosenberg, E. D., & Merk, R. 2008, *Space Sci. Rev.*, 138, 147
- Protopapa, S., Sunshine, J. M., Feaga, L. M., Kelley, M. S. P., A’Hearn, M. F., Farnham, T. L., Groussin, O., Besse, S., Merlin, F., & Li, J.-Y. 2014, *Icarus*, 238, 191
- Raghuram, S. & Bhardwaj, A. 2014, *A&A*, 566, A134
- Rauer, H., Biver, N., Crovisier, J., Bockelée-Morvan, D., Colom, P., Despois, D., Ip, W.-H., Jorda, L., Lellouch, E., Paubert, G., & Thomas, N. 1997, *Planet. Space Sci.*, 45, 799
- Rauer, H., Helbert, J., Arpigny, C., Benkhoff, J., Bockelée-Morvan, D., Boehnhardt, H., Colas, F., Crovisier, J., Hainaut, O., Jorda, L., Kueppers, M., Manfroid, J., & Thomas, N. 2003, *A&A*, 397, 1109
- Reach, W. T., Kelley, M. S., & Vaubaillon, J. 2013a, *Icarus*, 226, 777



—. 2013b, *Icarus*, 226, 777

Rettig, T. W., Tegler, S. C., Pasto, D. J., & Mumma, M. J. 1992, *ApJ*, 398, 293

Roemer, E. 1958, *PASP*, 70, 272

—. 1962, *PASP*, 74, 351

Romon-Martin, J., Delahodde, C., Barucci, M. A., de Bergh, C., & Peixinho, N. 2003, *A&A*, 400, 369

Rousselot, P. 2008, *A&A*, 480, 543

Rubin, M., Altwegg, K., Balsiger, H., Bar-Nun, A., Berthelier, J.-J., Bieler, A., Bochsler, P., Briois, C., Calmonte, U., Combi, M., De Keyser, J., Dhooghe, F., Eberhardt, P., Fiethe, B., Fuselier, S. A., Gasc, S., Gombosi, T. I., Hansen, K. C., Hässig, M., Jäckel, A., Kopp, E., Korth, A., Le Roy, L., Mall, U., Marty, B., Mousis, O., Owen, T., Rème, H., Sémon, T., Tzou, C.-Y., Waite, J. H., & Wurz, P. 2015, *Science*, 348, 232

Ruprecht, J. D., Bosh, A. S., Person, M. J., Bianco, F. B., Fulton, B. J., Gulbis, A. A. S., Bus, S. J., & Zangari, A. M. 2015, *Icarus*, 252, 271

Sarid, G., Prialnik, D., Meech, K. J., Pittichová, J., & Farnham, T. L. 2005, *PASP*, 117, 796

Schambeau, C. A., Fernández, Y. R., Lisse, C. M., Samarasinha, N., & Woodney, L. M. 2015, *Icarus*, 260, 60

Schmitt, B., Espinasse, S., Grim, R. J. A., Greenberg, J. M., & Klinger, J. 1989, in *ESA Special Publication*, Vol. 302, *Physics and Mechanics of Cometary Materials*, ed. J. J. Hunt & T. D. Guyenne

- Schulz, R. 2002, *A&A Rev.*, 11, 1
- Sekanina, Z. 1996, *A&A*, 314, 957
- . 1997, *Earth Moon and Planets*, 77, 147
- Sekanina, Z., Chodas, P. W., & Yeomans, D. K. 1994, *A&A*, 289, 607
- Sekanina, Z., Larson, S. M., Hainaut, O., Smette, A., & West, R. M. 1992, *A&A*, 263, 367
- Senay, M. C. & Jewitt, D. 1994, *Nature*, 371, 229
- Stansberry, J. A., Van Cleve, J., Reach, W. T., Cruikshank, D. P., Emery, J. P., Fernandez, Y. R., Meadows, V. S., Su, K. Y. L., Misselt, K., Rieke, G. H., Young, E. T., Werner, M. W., Engelbracht, C. W., Gordon, K. D., Hines, D. C., Kelly, D. M., Morrison, J. E., & Muzerolle, J. 2004, *Astroph. J. Supp.*, 154, 463
- Stern, S. A. 1989, *PASP*, 101, 126
- . 1995, *AJ*, 110, 856
- Stern, S. A., Cunningham, N. J., & Schindhelm, E. 2014, *AJ*, 147, 102
- Strazzulla, G., Pirronello, V., & Foti, G. 1983, *A&A*, 123, 93
- Tholen, D. J., Hartmann, W. K., Cruikshank, D. P., Lilly, S., Bowell, E., & Hewitt, A. 1988, *IAU Circ.*, 4554
- Thomas, N., Sierks, H., Barbieri, C., Lamy, P. L., Rodrigo, R., Rickman, H., Koschny, D., Keller, H. U., Agarwal, J., A’Hearn, M. F., Angrilli, F., Auger, A.-T., Barucci, M. A., Bertaux, J.-L., Bertini, I., Besse, S., Bodewits, D., Cremonese, G., Da Deppo, V., Davidsson, B., De Cecco, M., Debei, S., El-Maarry, M. R., Ferri, F., Fornasier, S., Fulle, M., Giacomini, L., Groussin, O., Gutierrez, P. J., Güttler, C., Hviid, S. F.,

- Ip, W.-H., Jorda, L., Knollenberg, J., Kramm, J.-R., Kührt, E., Küppers, M., La Forgia, F., Lara, L. M., Lazzarin, M., Moreno, J. J. L., Magrin, S., Marchi, S., Marzari, F., Massironi, M., Michalik, H., Moissl, R., Mottola, S., Naletto, G., Oklay, N., Pajola, M., Pommerol, A., Preusker, F., Sabau, L., Scholten, F., Snodgrass, C., Tubiana, C., Vincent, J.-B., & Wenzel, K.-P. 2015, *Science*, 347, aaa0440
- Trigo-Rodríguez, J. M., García-Hernández, D. A., Sánchez, A., Lacruz, J., Davidsson, B. J. R., Rodríguez, D., Pastor, S., & de Los Reyes, J. A. 2010, *MNRAS*, 409, 1682
- Weaver, H. A., Feldman, P. D., A’Hearn, M. F., & Arpigny, C. 1997, *Science*, 275, 1900
- Weaver, H. A. & Lamy, P. L. 1997, *Earth Moon and Planets*, 79, 17
- Weiler, M., Rauer, H., Knollenberg, J., Jorda, L., & Helbert, J. 2003, *A&A*, 403, 313
- Weissman, P. R. 1999, *Space Sci. Rev.*, 90, 301
- West, R. M. 1991, *A&A*, 241, 635
- Whipple, F. L. 1980, *AJ*, 85, 305
- Whitney, C. 1955, *ApJ*, 122, 190
- Womack, M., Festou, M. C., & Stern, S. A. 1997, *AJ*, 114, 2789
- Womack, M. & Stern, S. A. 1999, *Solar System Research*, 33, 187
- Womack, M., Wyckoff, S., & Ziurys, L. M. 1992, *ApJ*, 401, 728
- Woodney, L. M., A’Hearn, M. F., McMullin, J., & Samarasinha, N. 1997, *Earth Moon and Planets*, 78, 69
- Wyckoff, S., Wagner, R. M., Wehinger, P. A., Schleicher, D. G., & Festou, M. C. 1985, *Nature*, 316, 241

Yamamoto, T. 1985, A&A, 142, 31

Table 1: Sublimation Temperatures of Cometary Species

Species	Temperature <sup>a</sup> (K)
N <sub>2</sub>	22
CO	25
CH <sub>4</sub>	31
H <sub>2</sub> S	57
C <sub>2</sub> H <sub>2</sub>	57
H <sub>2</sub> CO	64
CO <sub>2</sub>	72
HC <sub>3</sub> N	74
NH <sub>3</sub>	78
CS <sub>2</sub>	78
SO <sub>2</sub>	83
CH <sub>3</sub> CN	91
HCN	95
CH <sub>3</sub> OH	99
H <sub>2</sub> O	152

---

<sup>a</sup>(Yamamoto 1985; Sekanina 1996)

Table 2: Representative Gaseous Production Rates in Three Comets Beyond 4 AU

Comet	Molecule	r (AU)	Q (number/s)	Reference
29P	CN	5.8	$8.0 \times 10^{24}$	(Cochran & Cochran 1991)
29P	CO	5.7 - 6.2	$1\text{-}7 \times 10^{28}$	various <sup>a</sup>
29P	H <sub>2</sub> O	6.2	$6.3 \times 10^{27}$	(Ootsubo et al. 2012)
29P	CO <sub>2</sub>	6.2	$<3.5\text{e}26$	(Ootsubo et al. 2012)
29P	HCN	6.3	$< 1.4 \times 10^{27}$	(Paganini et al. 2013)
29P	CH <sub>3</sub> OH	6.3	$<9.3 \times 10^{27}$	(Paganini et al. 2013)
29P	CH <sub>4</sub>	6.3	$<1.3 \times 10^{27}$	(Paganini et al. 2013)
Chiron	CN	11.3	$3.7 \times 10^{25}$	(Bus et al. 1991)
Chiron	CO	8.5	$1.3 \times 10^{28}$	(Womack & Stern 1999), recalculated
Chiron	H <sub>2</sub> O (via OH)	8.5	$<4 \times 10^{30}$	(Parker et al. 1997)
Chiron	H <sub>2</sub> S	8.5	$<2.1 \times 10^{27}$	(Rauer et al. 1997)
Chiron	H <sub>2</sub> CO	8.5	$<4.2 \times 10^{26}$	(Rauer et al. 1997)
Hale-Bopp	CN	6.8	$6 \times 10^{25}$	(Fitzsimmons & Cartwright 1996)
Hale-Bopp	CN	9.8	$0.9 \times 10^{25}$	(Rauer et al. 2003)
Hale-Bopp	CO	6.8	$1.8 \times 10^{28}$	(Jewitt et al. 1996)
Hale-Bopp	H <sub>2</sub> O	4.8	$2.0 \times 10^{28}$	(Weaver et al. 1997)
Hale-Bopp	CO <sub>2</sub>	4.6	$1.3 \times 10^{28}$	(Crovisier 1997)
Hale-Bopp	HCN	4.8	$2 \times 10^{26}$	(Jewitt et al. 1996)
Hale-Bopp	CH <sub>3</sub> OH	5.0	$3.3 \times 10^{27}$	(Womack et al. 1997)
Hale-Bopp	H <sub>2</sub> CO	4.1	$5.8 \times 10^{26}$	(Biver et al. 1999)
Hale-Bopp	C <sub>3</sub>	7.0	$\leq 0.6 \times 10^{25}$	(Rauer et al. 2003)

<sup>a</sup>The range of CO production rates typically observed is listed, taken from Senay & Jewitt (1994); Crovisier et al. (1995); Festou et al. (2001); Gunnarsson et al. (2008); Paganini et al. (2013)

Table 3: CN/CO production rate ratios in three distant comets

Comet	$r$ (AU)	$Q(\text{CN})/Q(\text{CO})$	Reference
Chiron	11, 8.5	0.0025	Bus et al. (1991); Womack & Stern (1999)
29P	5.8	0.0003	Cochran & Cochran (1991); Gunnarsson et al. (2008) <sup>a</sup>
Hale-Bopp	6.8	0.0033	Fitzsimmons & Cartwright (1996); Jewitt et al. (1996)
Hale-Bopp	6.0	0.0040	Rauer et al. (1997); Biver et al. (2002)

<sup>a</sup>This ratio for 29P may typically be significantly lower, as CN is rarely observed in this comet.

Table 4: Ratios of CO<sub>2</sub>/CO production rates in distant comets

Comet	$r$ (AU)	$Q(\text{CO}_2)/Q(\text{CO})$	Reference
29p	6.2	$<0.0125$	Ootsubo et al. (2012)
Hale-Bopp	4.6	0.10	Crovisier (1997)
Hale-Bopp	4.9	0.19	Crovisier (1997)
Hale-Bopp	4.0	0.55	Weaver et al. (1997)
Hale-Bopp	3.89	0.10	Crovisier (1997)



Table 5: CO Production Rates in Comet 29P

Date	r (AU)	$Q^a$ ( $\times 10^{28}$ molecules $s^{-1}$ )
25-Feb-16	5.96	$5.3 \pm 1.3$
26-Feb-16	5.96	$3.8 \pm 0.9$
28-Feb-16	5.96	$5.1 \pm 1.3$
29-Feb-16	5.96	$2.5 \pm 0.6$
1-Mar-16	5.96	$2.8 \pm 0.7$
3-Mar-16	5.96	$2.6 \pm 0.7$
21-Mar-16	5.95	$3.2 \pm 0.8$
28-Mar-16	5.95	$2.6 \pm 0.7$
31-Mar-16	5.95	$1.0 \pm 0.2$
9-Apr-16	5.95	$0.9 \pm 0.2$
15-Apr-16	5.95	$0.8 \pm 0.2$
24-Apr-16	5.94	$1.0 \pm 0.2$
29-May-16	5.93	$1.0 \pm 0.3$

---

<sup>a</sup>Production rates derived from observations of the CO J=2-1 line using the Arizona Radio Observatory 10-m Submillimeter Telescope (SMT). Full details in Wierchos et al., in preparation.

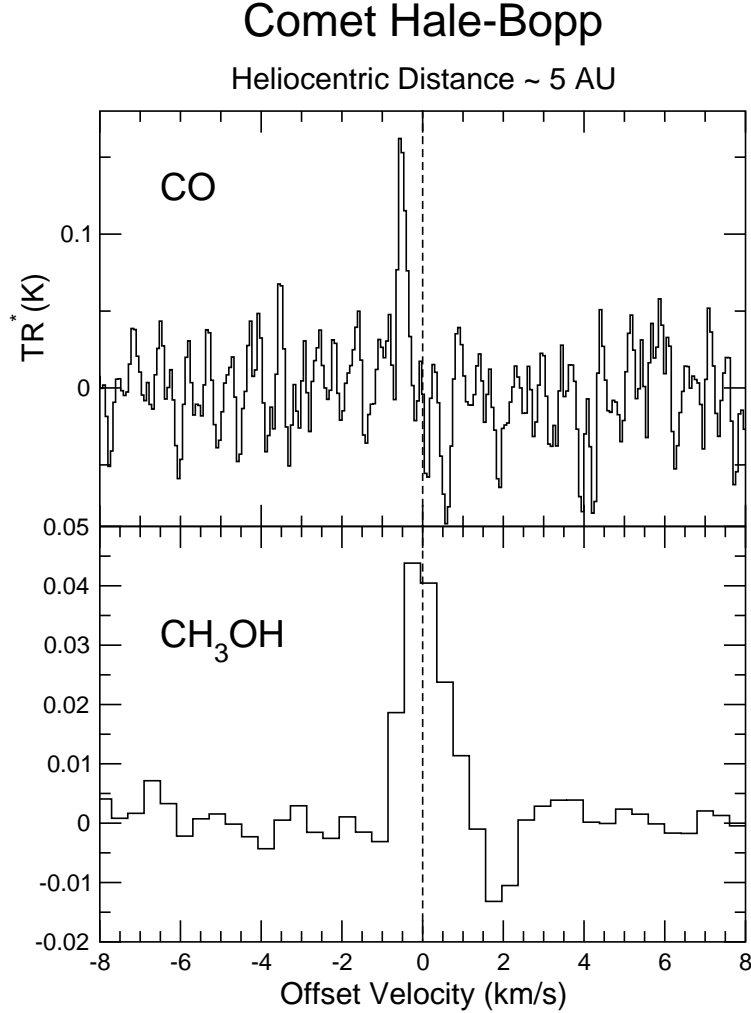


Fig. 1.— Spectra of CO and CH<sub>3</sub>OH emission from comet C/1995 O1 Hale-Bopp at 5 AU, pre-perihelion, obtained with the NRAO 12-m telescope. The CO J=2-1 spectrum was obtained at 230 GHz on 1996 March 31 with 49 kHz/channel resolution, which corresponds to 0.06 km/s/channel; the methanol emission was obtained at 145 GHz on 1996 Apr 16 with 195 kHz/channel resolution, which corresponds to 0.40 km/s/channel. The dotted line indicates the comet’s rest frame velocity. As the figure shows, the CO emission is blue-shifted from the ephemeris velocity of the comet and has a very narrow line-width. In contrast, the methanol emission has no measurable shift from the comet’s velocity and has a broader line-width. This difference can be explained if CO emission originates from within the cold comet nucleus and the methanol escapes from hot grains in the coma.

### CO Production Rates in 3 Distant Comets

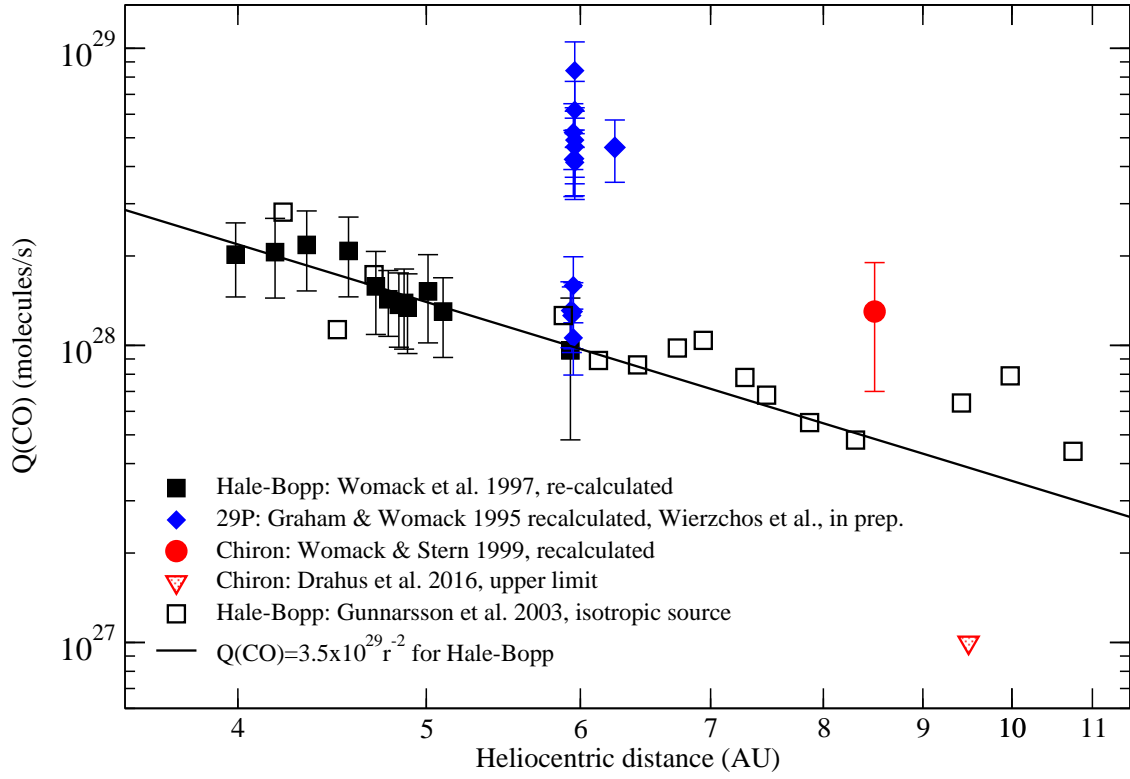


Fig. 2.— CO production rates from three distant comets are plotted against heliocentric distance. The observations of Hale-Bopp and 29P are consistent with a nominal production rate of  $Q(\text{CO}) = 3.5 \times 10^{29} r^{-2}$  superimposed with sporadic outbursts.

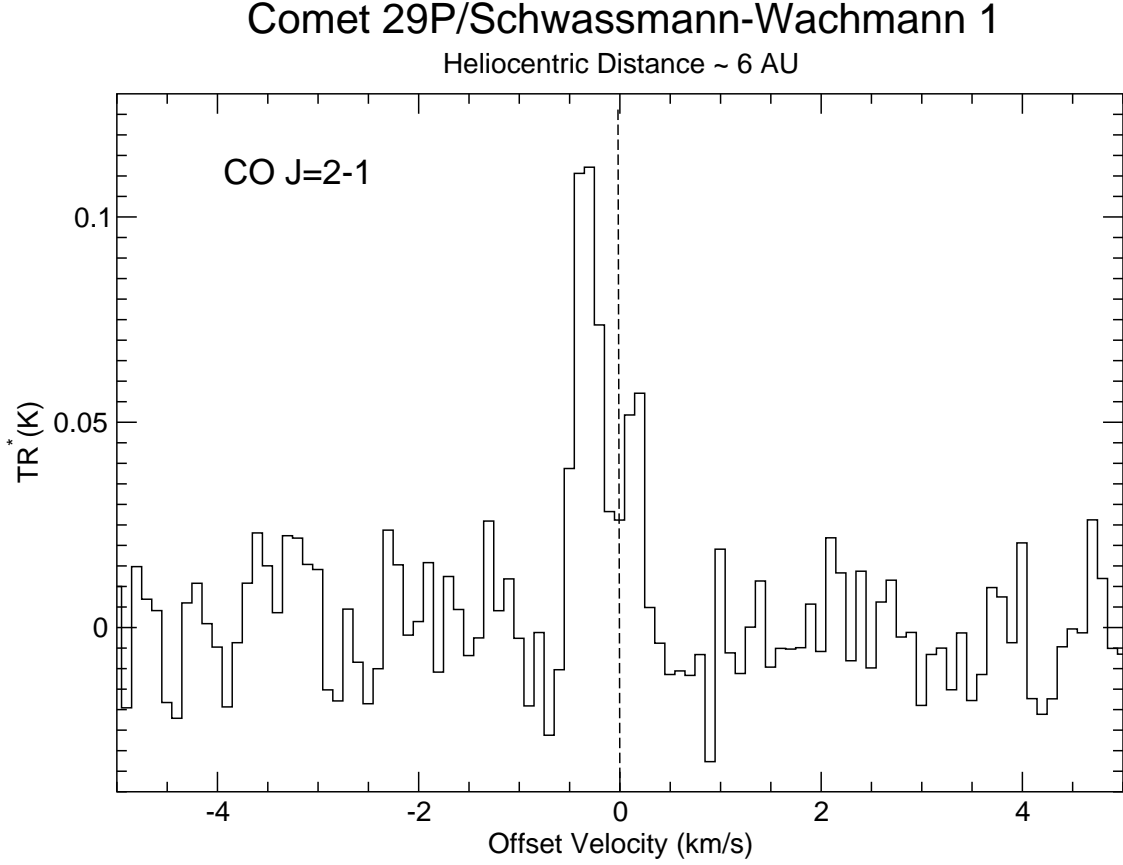


Fig. 3.— Spectrum of the CO J=2-1 rotational line in comet 29P/Schwassmann-Wachmann 1 obtained from 1995 Dec 9–11 UT with the NRAO 12-m telescope (Graham & Womack 1995). The spectral resolution was 100 kHz, which corresponds to 0.13 km/s per channel. The dotted line indicates the comet’s rest frame velocity. Two narrow velocity components are seen in this spectrum and in many other observations of this comet.

### Specific Production Rates for CO in Distant Comets

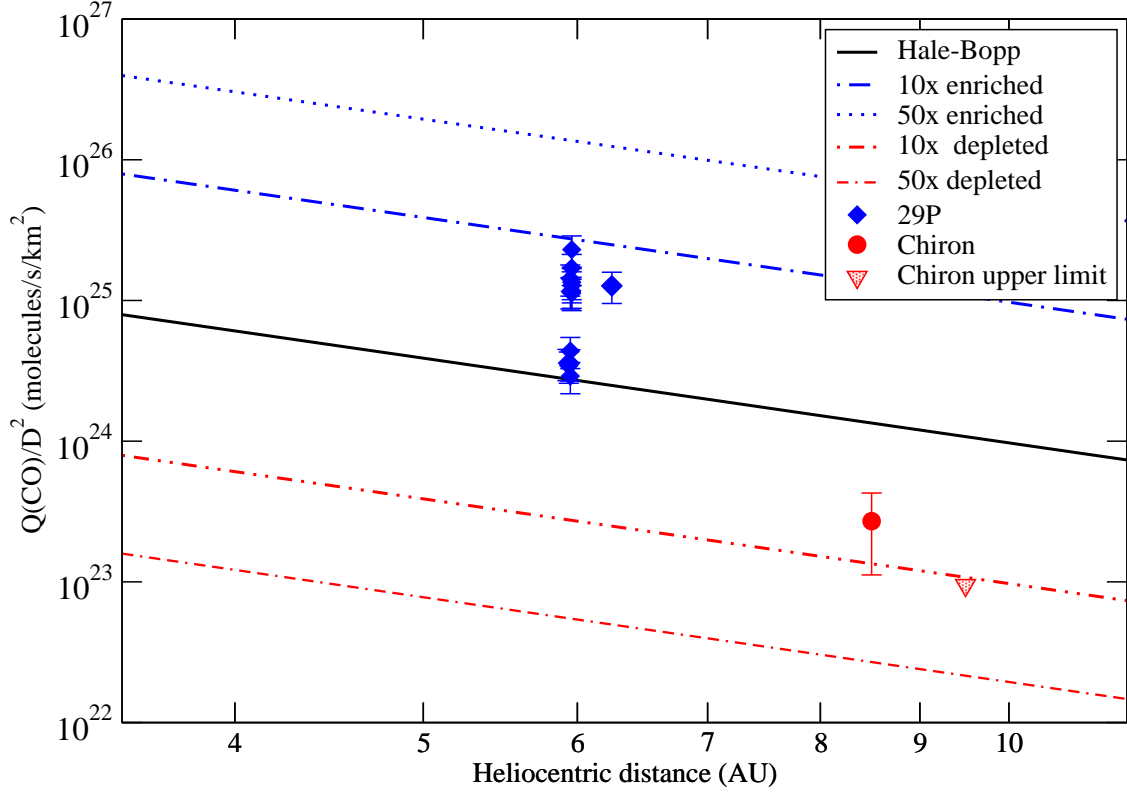


Fig. 4.— Specific production rates,  $Q(\text{CO})/D^2$ , for distant comets. The solid line is the specific production rate derived for Hale-Bopp, assuming  $Q(\text{CO})=3.5 \times 10^{29}r^{-2}$ , and diameter  $D_{\text{Hale-Bopp}}=60\text{km}$ . Values for Chiron and 29P are plotted assuming production rates from Figure 2 and  $D_{\text{Chiron}}=218\text{km}$  and  $D_{29P}=60\text{ km}$ . This plot shows that, when adjusted for surface area and heliocentric distance, 29P (in non-outbursting mode) produces CO at approximately the same rate as, and up to ten times larger than, Hale-Bopp. In contrast, Chiron produces at least 5-15 times less CO than Hale-Bopp. This may indicate that 29P entered its current orbit more recently than many models predict, and that Chiron is significantly depleted in CO over its initial chemical composition.